Synthesis, crystal structures and optical properties of mercury(II) halide compounds with (E)-N-(pyridin-2-ylmethylidene)arylamines: Effect of ligand R-group upon structure

Basu Baul, Tushar S ; Kundu, Sajal ; Höpfl, Herbert ; Tiekink, Edward R T ; Linden, Anthony

Abstract: A systematic series of seven mercury compounds of (E)-N-(pyridin-2-ylmethylidene)arylamine (L), where L is a variously R substituted ligand, with the formulations [HgX2L]2: X = Cl; R = 4-CH2CH3 (4), 4-OCH2CH3 (5), 4-Cl (6), 2-CO2CH3 (7), or 4-CO2CH3 (8); X = Br; R = 4-CO2CH3 (9a) and [HgX2L]: X = Br; R = 4-CO2CH3 (9b) and X = I; R = 4-CO2CH3 (10), were synthesized. All compounds have been structurally characterized by single-crystal X-ray diffraction studies and their spectroscopic (IR, NMR, UV–Vis and fluorescence) properties are described. The structural analyses reveal that compounds 4–9a are centrosymmetric binuclear compounds while compounds 9b (a polymorph of the binuclear compound 9a) and 10 are mononuclear compounds. The HgCl2 compounds are more likely to dimerize via Hg Cl bridges complexed with (E)-N-(pyridin-2-ylmethylidene)arylamine ligands compared with their HgBr2 and HgI2 analogs. This feature of the structural chemistry is correlated with the enhanced Lewis acidity of the mercury in the HgCl2 compounds. Moderating the electronegativity of the substituents in L is shown to influence the strength of the Hg–N(imino) bond in HgCl2L compounds.

DOI: https://doi.org/10.1016/j.poly.2013.03.025

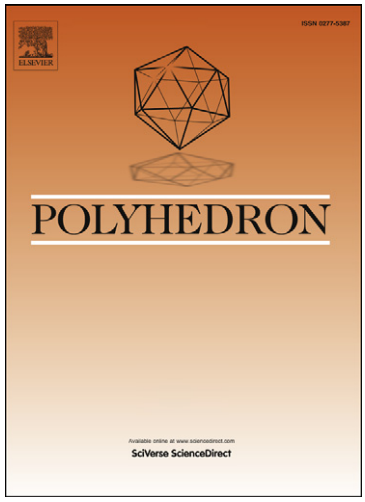

Synthesis, crystal structures and optical properties of mercury(II) halide compounds with (E)-*N*-(pyridin-2-ylmethylidene)arylamine: Effect of ligand R-group upon structure

Tushar S. Basu Baul, Sajal Kundu, Herbert Höpfl, Edward R.T. Tiekink, Anthony Linden

PII: S0277-5387(13)00226-X
DOI: http://dx.doi.org/10.1016/j.poly.2013.03.025
Reference: POLY 10015

To appear in: *Polyhedron*

Received Date: 7 February 2013
Accepted Date: 13 March 2013

Please cite this article as: T.S. Basu Baul, S. Kundu, H. Höpfl, E.R.T. Tiekink, A. Linden, Synthesis, crystal structures and optical properties of mercury(II) halide compounds with (E)-*N*-(pyridin-2-ylmethylidene)arylamine: Effect of ligand R-group upon structure, *Polyhedron* (2013), doi: http://dx.doi.org/10.1016/j.poly.2013.03.025

Synthesis, crystal structures and optical properties of mercury(II) halide compounds with (*E*)-*N*-(pyridin-2-ylmethylidene)arylamine: Effect of ligand R-group upon structure

Tushar S. Basu Baul[a,*], Sajal Kundu [a], Herbert Höpfl[b], Edward R. T. Tiekink[c,*], Anthony Linden[d]

[a]*Department of Chemistry, North-Eastern Hill University, NEHU Permanent Campus, Umshing, Shillong 793 022, India*

[b]*Centro de Investigaciones Químicas, Universidad Autónomadel Estado de Morelos, Av. Universidad 1001, 62209 Cuernavaca, Mexico*

[c]*Department of Chemistry, University of Malaya, 50603 Kuala Lumpur, Malaysia*

[d]*Institute of Organic Chemistry, University of Zurich, Winterthurerstrasse 190, CH-8057 Zurich, Switzerland*

ABSTRACT

A systematic series of seven mercury compounds of (*E*)-*N*-(pyridin-2-ylmethylidene)arylamine (L), where L is a variously R substituted ligand, with the formulations $[HgX_2L]_2$: X = Cl; R = 4-CH_2CH_3 (**4**), 4-OCH_2CH_3 (**5**), 4-Cl (**6**), 2-CO_2CH_3 (**7**), or 4-CO_2CH_3 (**8**); X = Br; R = 4-CO_2CH_3 (**9a**) and $[HgX_2L]$: X = Br; R = 4-CO_2CH_3 (**9b**) and X = I; R = 4-CO_2CH_3 (**10**), were synthesized. All compounds have been structurally characterized by single-crystal X-ray diffraction studies and their spectroscopic (IR, NMR, UV-Vis and fluorescence) properties are described. The structural analyses reveal that compounds **4**-**9a** are centrosymmetric binuclear compounds while compounds **9b** (a polymorph of the binuclear compound **9a**) and **10** are mononuclear compounds. The $HgCl_2$ compounds are more likely to dimerize *via* Hg...Cl bridges complexed with (*E*)-*N*-(pyridin-2-ylmethylidene)arylamine ligands compared with their $HgBr_2$ and HgI_2 analogues. This feature of the structural chemistry is correlated with the enhanced Lewis acidity of the mercury in the $HgCl_2$ compounds. Moderating the electronegativity of the substituents in L is shown to influence the strength of the Hg–N(imino) bond in $HgCl_2L$ compounds.

Keywords: Mercury / (*E*)-*N*-(pyridin-2-ylmethylidene)arylamine / *N*,*N*- donor ligands / Spectroscopy / Structure elucidation / Crystal structure

**Corresponding authors. E-mail:* basubaul@nenu.ac.in, basubaulchem@gmail.com; Fax: +91-3642721000; Tel: +91-3642722626 (T. S. Basu Baul); *E-mail:* Edward.Tiekink@gmail.com; Fax: +60 3 7967 4193; Tel: +60 3 7967 6775 (E. R. T. Tiekink).

1. Introduction

The main group elements are typically defined as the set of s and p block elements, plus zinc, cadmium, and mercury [1]. Group 12 compounds are particularly challenging to separate into main group versus transition metal-type complexes, as zinc tends to behave more as a transition metal in terms of reactivity and coordination preferences. However, the Hg(II) ion typically adopts either two-coordinate, linear geometries or distorted tetrahedral, nearly disphenoidal-type of geometries, and therefore, tends to have much more in common with main group elements owing to this propensity. Main group elements have unique coordination preferences and electronic properties, and thereby present opportunities for the preparation of novel structures with new and interesting characteristics [1-3]. Moreover, crystal engineering represents a fascinating and constantly growing field which aims at understanding intermolecular interactions and, exploiting these analytical results, at the synthesis of new structures with desired properties [4,5]. In line with the above, we recently reported on the syntheses and the self-assembly of some Hg(II) compounds of composition $[HgX_2L]$, $[HgX_2L]_2$, $[HgX_2L]_n$ and $\{[HgX_2L]_2\}_n$ where X = chloride, bromide, iodide, nitrates, and azides, and L is a (*E*)-*N*-(pyridin-2-ylmethylidene)arylamine [6]. The interplay between the three components Hg, X, and L greatly influences the observed structure type and patterns of self-assembly as monomeric tetrahedral, dimeric and polymeric trigonal bipyramidal, and polymeric octahedral geometries were encountered. The results indicated that dimeric structures with a trigonal bipyramidal geometries (Scheme 1a) is prevalent among the reaction products of HgX_2 with L. Literature surveys have shown that different coordination numbers and geometries of the mercury centre have been found when a remote ligand substituent is altered. This phenomenon is not restricted to mercury alone, but may be found in many other main group elements systems as well [7-9]. As a part of

an on-going investigation into the factor(s) that influence molecular geometry in chemically similar compounds, the synthesis and structures of eight new mercury(II) compounds are presented in which X and the substituents (R) on the phenyl ring of L have been varied systematically (Scheme 1b). Six dimers and two mononuclear compounds, one of which is a polymorph of a dimer, have been structurally characterized by single-crystal X-ray diffraction and spectroscopic (IR, NMR, UV-Vis and fluorescence) methods.

94

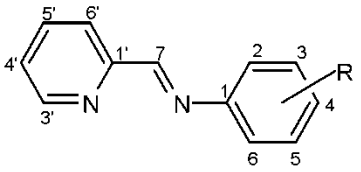

L

R = H (L^1), 2-CH_3 (L^2), 3-CH_3 (L^3), 4-CH_3 (L^4)

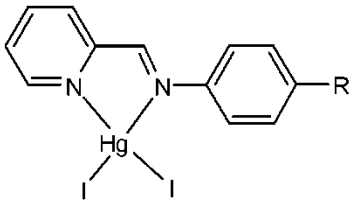

(**i**) HgI_2L

R = H; R = CH_3 (**3**)

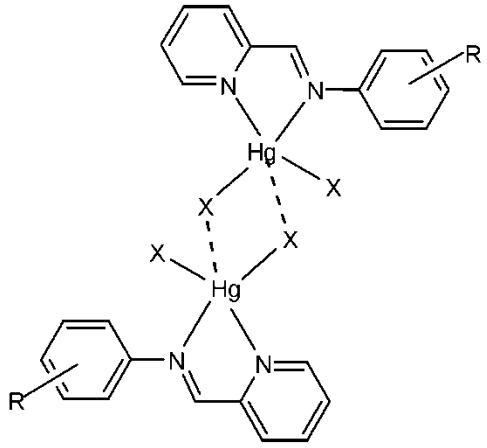

$[HgX_2L]_2$

(**ii**) R = H, X = Cl; R = H, X = Br; R = 2-CH_3, X = Cl; R = 3-CH_3, X = Cl; R = 4-CH_3, X = Cl (**1**); R = 4-CH_3, X = Br (**2**)

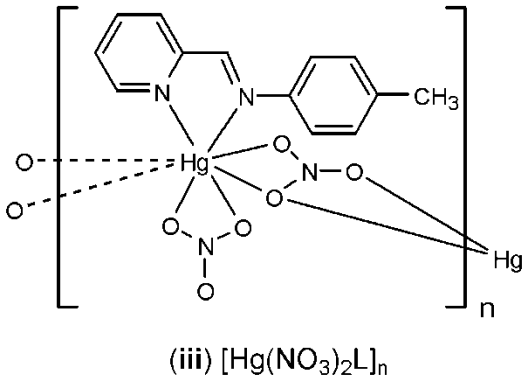

(**iii**) $[Hg(NO_3)_2L]_n$

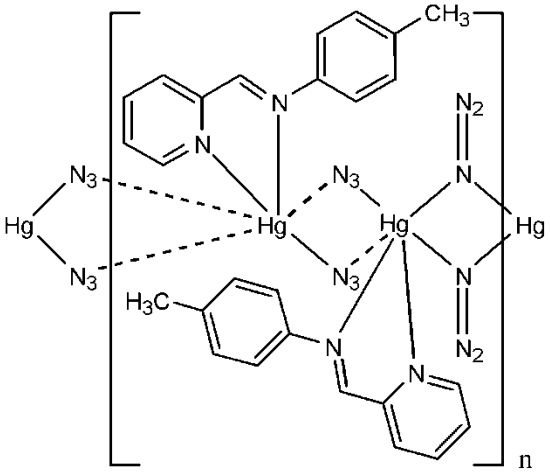

(**iv**) $\{[Hg(N_3)_2L]_2\}_n$

95

96 Scheme 1a. Various structural motifs (**i**-**iv**) observed in mercury(II) compounds with (*E*)-*N*-(pyridin-2-

97 ylmethylidene)arylamine, L (taken from ref. 6).

98

99

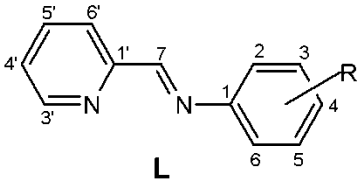

L

R = 4-CH_2CH_3 (L^1), 4-OCH_3CH_2 (L^2), 4-Cl (L^3), 2-CO_2CH_3 (L^4), 4-CO_2CH_3 (L^5)

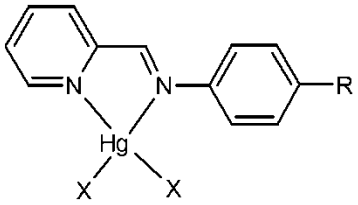

HgX_2L

R = 4-CO_2CH_3, X = Br (**9b**); 4-CO_2CH_3, X = I (**10**)

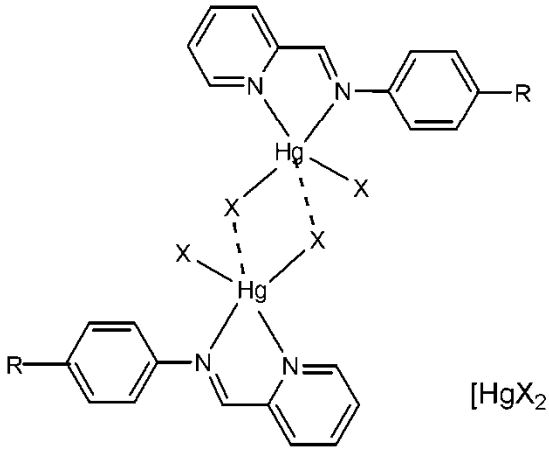

$[HgX_2L]_2$

R = 4-CH_2CH_3, X = Cl (**4**); R = 4-OCH_2CH_3, X = Cl (**5**); R = 4-Cl, X = Cl (**6**); R = 4-CO_2CH_3, X = Cl (**8**); R = 4-CO_2CH_3, X = Br (**9a**)

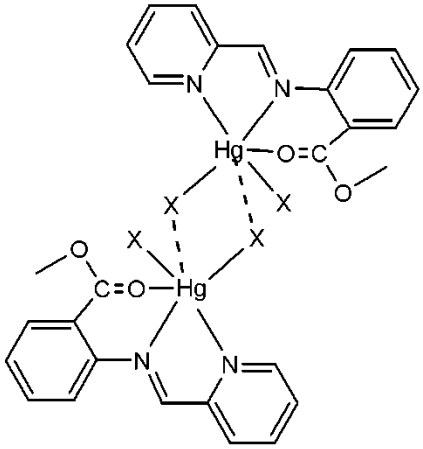

R = 2-CO_2CH_3, X = Cl (**7**)

Scheme 1b. The L ligands used and the investigated compounds **4**-**10**.

2. Results and Discussion

2.1. Syntheses

A systematic series of seven mercury compounds with the general stoichiometry HgX_2L has been prepared, where X is a chloride, bromide or iodide, and L is a 4-R substituted Schiff base ligand, (*E*)-*N*-(pyridin-2-ylmethylidene)arylamine where R = CH_2CH_3, OCH_2CH_3, Cl or CO_2CH_3 (**4**-**6**, **8**-**10**) while compound **7** incorporates a 2-R substituted variant of L with R = CO_2CH_3, *i.e.* (*E*)-methyl-2-((pyridin-2-ylmethylidene)amino)benzoate, in order to observe the influence of *ortho*-substitution on the mercury coordination geometry preferences. In alcohol, one equivalent of HgX_2 reacts rapidly with one equivalent of L (generated *in situ* from pyridine-

2-carboxaldehyde and a substituted aniline) to give a yellow precipitate from which mercury compounds of the formula $[HgX_2L]_2$ (**4**-**8** and **9a**) and $[HgX_2L]$ (**9b** and **10**) were isolated and each of which has been characterized crystallographically. Some results for mercury compounds **1**-**3** (see Scheme 1a; L = 4-CH_3, *i.e*. (*E*)-4-methyl-*N*-(pyridin-2-ylmethylidene)aniline and X = Cl (**1**), Br (**2**) and I (**3**)) are also included herein for comparison; their syntheses and crystal structures having been reported previously [6]. The mercury compounds are insoluble in the reaction medium and can be re-crystallized using a large volume of acetonitrile (refer to work-up procedure) to provide crystals suitable for X-ray crystallography. Two polymorphs of **9** (**9a** and **9b**) were characterized from two different batches of crystals, each obtained from acetonitrile solution. The results of the crystal structure determinations of **4**-**10** (see below) are consistent with the chemical and spectroscopic analyses, giving clear evidence of the formation of the 1:1 adducts between the bidentate N-donors and HgX_2. Compounds **4**-**10** are all air-stable and behave as non-electrolytes in acetonitrile solution.

2.2. IR, NMR, UV-Vis and Fluorescence spectroscopy

The infrared spectra of compounds **4**-**10** are very similar and the IR assignments of selected diagnostic bands are included in the *Experimental section*. The compounds display a moderately intense IR band in the region 1620-1650 cm^{-1} which is assigned to the ν_{asym}(C(H)=N) stretch of the coordinated Schiff base ligands [6]. In addition, well resolved-sharp bands of variable intensity observed in the regions 1600-1550, 1490-1480 and 1400-1430 cm^{-1} are assigned to the coordinated pyridine ring [6,10-11]. These data are in agreement with the coordination of imino- and pyridine-N atoms to the mercury atom [6]. On the other hand, a very strong band in the range 1700-1712 cm^{-1} is detected in compounds **7**-**10** which has been assigned to ν_{asym}(OCO). The lowering of ν_{asym}(OCO) band in **7** (1700 cm^{-1}) compared to its *p*-analogues **8**-**10** is suggestive of

coordination of ν(C=O→Hg). The ^{1}H NMR spectra were recorded in DMSO-d_6 solution which displayed the expected signals which were generally broad. Coupling constants of some signals for compounds **5**, **6** and **10** could not be derived with certainty owing to the complicated splitting yet the multiplicity patterns could be delineated.

Table 1 summarizes the UV-Vis and fluorescent properties of compounds **4**-**10** along with the previously reported data for **1**-**3** [6]. The electronic spectra in acetonitrile solutions exhibit a coalesced absorption band in the range of 320 to 350 nm (Fig. 1) which is possibly a result of overlap of intramolecular charge transfer transitions with a weak band due to MLCT transition from Hg(II)→ π^* (ligand), as noted earlier for the cognate systems [6]. The steady-state fluorescence studies have been employed as independent evidence of complexation between the ligand and the mercury ions. In acetonitrile solution, the compounds all display broad emission bands at around λ_{max} = 410 nm along with a shoulder at ~ 430 nm, except for **7**, which displayed a distinct absorption at 395 nm, when they are excited at their respective absorption maxima (Fig. 2), indicating the charge transfer nature of the transitions [6]. In general, all compounds show very low fluorescent quantum yield (ϕ_F) [6]. No change in ϕ_F was perceived when nuclear substituents in the compounds were varied from 4-CH_3 (**1**-**3**) to 4-CH_2CH_3 (**4**), 4-OCH_2CH_3 (**5**), 4-Cl (**6**), or 4-CO_2CH_3 (**8**-**10**). However, an appreciable change was noticed in the case of compound **7**, which was shown to feature a close Hg...O interaction.

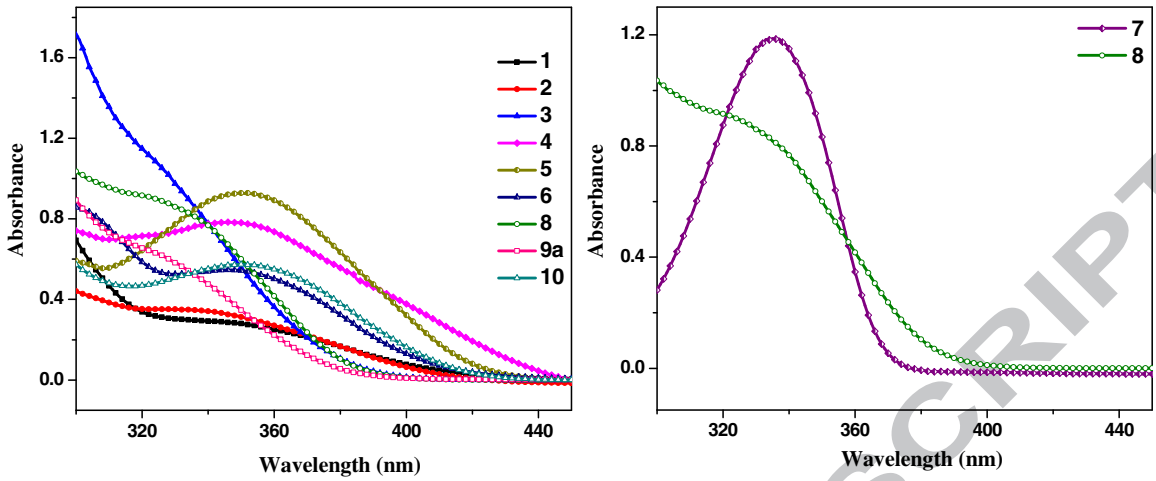

164

165 Fig. 1. UV–Vis spectra of compounds **1**-**10** in acetonitrile (concentration 10^{-5}M). Spectra of

166 compounds **7** and **8**, with CO_2CH_3 substituents, are shown separately for convenience.

167

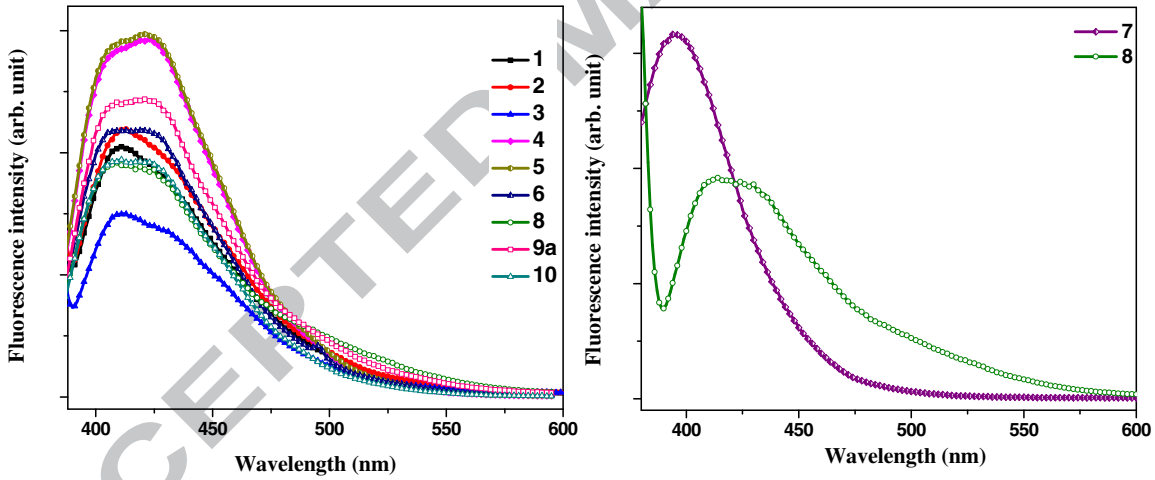

168

169 Fig. 2. Fluorescence spectra of compounds **1**-**10** in acetonitrile (concentration ~10^{-5}M) obtained

170 by excitation at the respective absorption maxima (refer to Table 1). Spectra of compounds **7** and

171 **8**, with CO_2CH_3 substituents, are shown separately for convenience.

172
173

174

175 *2.3. Molecular structures*

The crystal and molecular structures of solvent-free **4**-**10** have been determined with crystal data and selected geometric parameters for these collated in Tables 2 and 3, respectively. The $HgCl_2$ structures with 4-substituted rings are discussed first and related to their $HgBr_2$ and HgI_2 counterparts where applicable. The sole example of a characterized HgX_2 structure with a 2-substituted aryl ring is discussed last. The molecular structures are uniformly zero-dimensional, being mono- or, usually, bi-nuclear.

The binuclear molecule of $[HgCl_2L^1]_2$ (**4**, Fig. 3) is the archetype for most of the molecules described herein and, as such, is described in more detail. The immediate environment for the mercury atom is defined by the pyridyl-N1 and imino-N2 atoms derived from the chelating (*E*)-4-ethyl-*N*-(pyridin-2-ylmethylidene)aniline ligand and two chlorido ligands. The Hg–N(pyridyl) bond length is significantly shorter than the Hg–N(imino) bond length, a trend that is maintained in all molecules in the present study. The resulting five-membered HgN_2C_2 chelate ring is planar with the root-mean-square (r.m.s.) deviation of the fitted atoms being 0.015 Å; the maximum deviation is 0.015(7) Å for the C6 atom. Overall, the chelating ligand exhibits a small twist from planarity with the dihedral angle between the planes of the terminal rings being 10.8(4)°. Molecules self-associate over a centre of inversion *via* unsymmetric μ_2-chlorido bridges, the difference in Hg–Cl1 and Hg–Cl1^i bond lengths, Δ(Hg-Cl1), being 0.47 Å; symmetry operation i: 1-x, 1-y, 1-z. As anticipated, the terminally coordinated chlorido atom forms a significantly shorter Hg–Cl bond compared with those formed by the bridging chlorido atoms. The coordination geometry is highly distorted owing in part to the restricted bite angle of the chelating ligand (70.28(18)°) and the disparate Hg-Cl bond lengths. The Cl_3N_2 donor set defines a coordination geometry intermediate between square pyramidal and trigonal bipyramidal as

198 quantified by the value of the trigonality index, τ, = 0.42 which compares to the τ values of 0.0
199 and 1.0 for ideal square pyramidal and trigonal bipyramidal geometries, respectively [12].

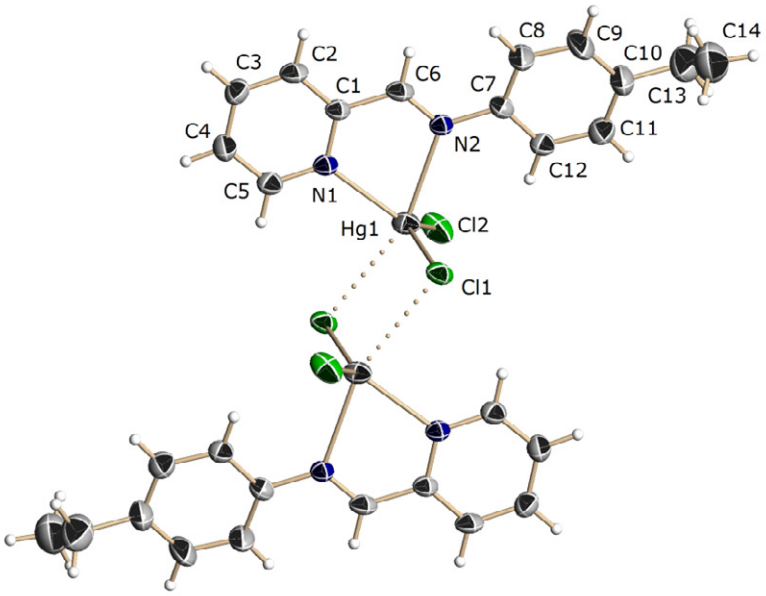

200

201 Fig. 3. Perspective view of binuclear $[HgCl_2L^1]_2$ **4**. Displacement ellipsoids are drawn at the 30%
202 probability level and unlabelled atoms are related by the symmetry operation 1-x, 1-y, 1-z.

203

204 To a first approximation, the binuclear molecules of $[HgCl_2L^2]_2$ (**5**, Fig. 4), $[HgCl_2L^3]_2$ (**6**,
205 Fig. 5) and $[HgCl_2L^5]_2$ (**8**, Fig. 6) resemble that just described for **4**. The dimeric structures are
206 centrosymmetric and feature distorted penta-coordinate geometries with τ being 0.39, 0.44 and
207 0.16, respectively. The chelating ligands in **5**, **6** and **8** range from planar in **5** to significantly
208 twisted in **6** and **8** as seen in the dihedral angles between the planes of the six-membered rings of
209 1.3(2), 18.8(3) and 24.41(14)°, respectively. Systematic variations in the geometric parameters
210 are observed and these are correlated with the enhanced electronegativities of the substituents in
211 the 4-position of the aryl rings, *i.e.* OCH_2CH_3 (**5**), Cl (**6**) and CO_2CH_3 (**8**), compared with
212 CH_2CH_3 in **4**. As a general trend, as the electronegativity of the substituent increases, the Hg–

N(imino) bond lengths elongate with a concomitant reduction in the Hg–N(pyridyl) distances, reflecting a reduction in the basicity of the imino-N2 atom and a reduced tendency for coordination. This is echoed in the Δ(Hg–N) values which vary from a small 0.13 Å for **4** to a maximum of 0.28 Å for **8**. There are also variations in the Hg–Cl bond lengths so that a general trend towards elongation of both Hg–Cl1 and Hg–Cl2 bonds correlates with an increase in asymmetry in the mode of coordination of the chelate. It is noted for **8** that the μ_2-chlorido bridges are the most symmetric, *i.e.* Δ(Hg–Cl1) = 0.34 Å.

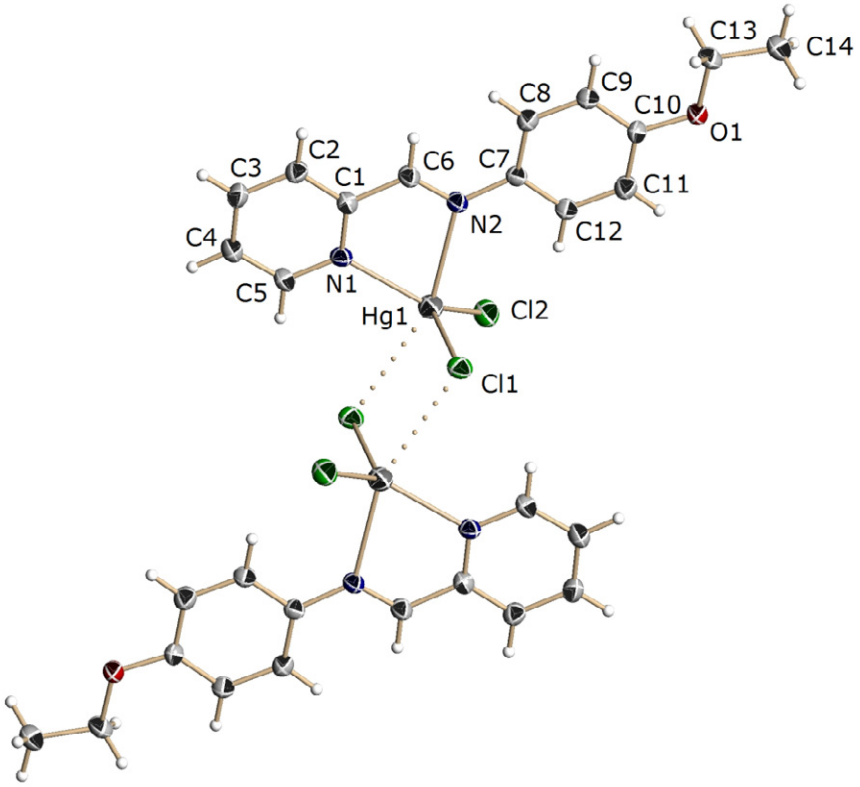

Fig. 4. Perspective view of binuclear $[HgCl_2L^2]_2$ **5**. Displacement ellipsoids are drawn at the 50% probability level and unlabelled atoms are related by the symmetry operation -x, -y, -z.

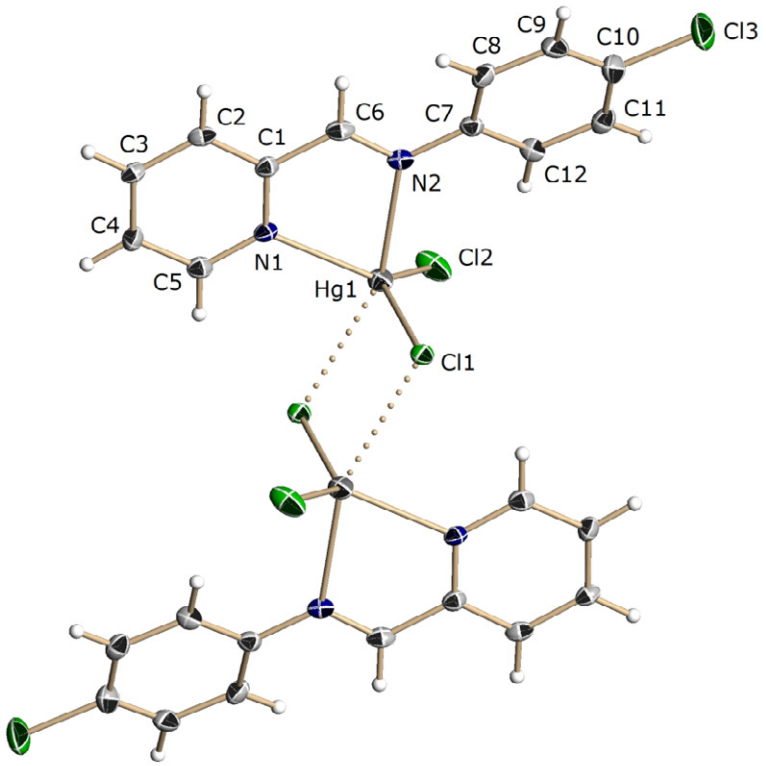

224

225 Fig. 5. Perspective view of binuclear $[HgCl_2L^3]_2$ **6**. Displacement ellipsoids are drawn at the 30%

226 probability level and unlabelled atoms are related by the symmetry operation -x, 1-y, -z.

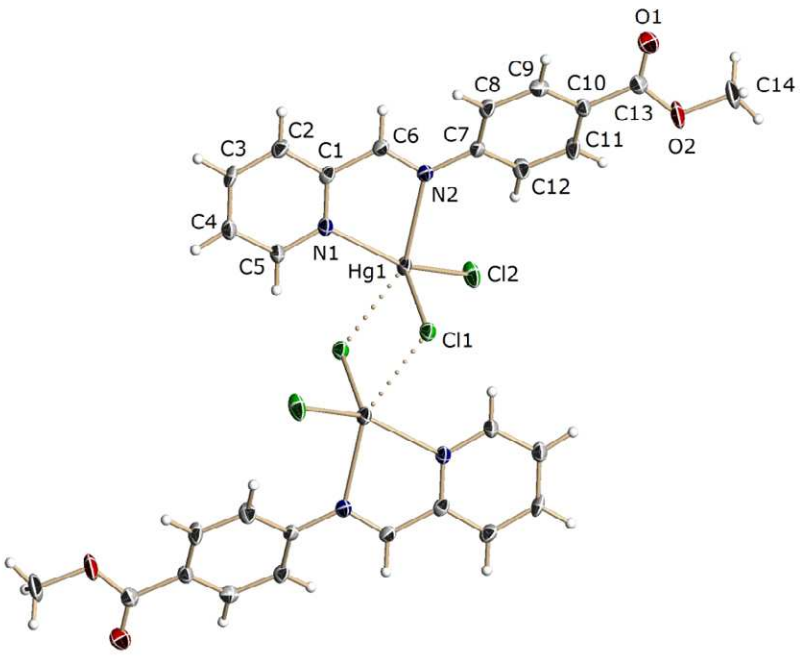

227

Fig. 6. Perspective view of binuclear $[HgCl_2L^5]_2$ **8**. Displacement ellipsoids are drawn at the 30% probability level and unlabelled atoms are related by the symmetry operation -x, 1-y, -z.

It also proved possible to grow crystals of the 1:1 compounds of each of $HgBr_2$ and HgI_2 with L^5. Curiously, two polymorphic forms of the 1:1 compound with $HgBr_2$, namely $[HgBr_2L^5]_2$ (**9a**) and $[HgBr_2L^5]$ (**9b**) were isolated, both from slow evaporation of an acetonitrile solution. Polymorphs **9a** and **9b** each crystallize in the triclinic space group *P1* and have very similar unit cell characteristics (Table 2). The key difference between them is the formation of intermolecular Hg...Br interactions only in the case of **9a**.

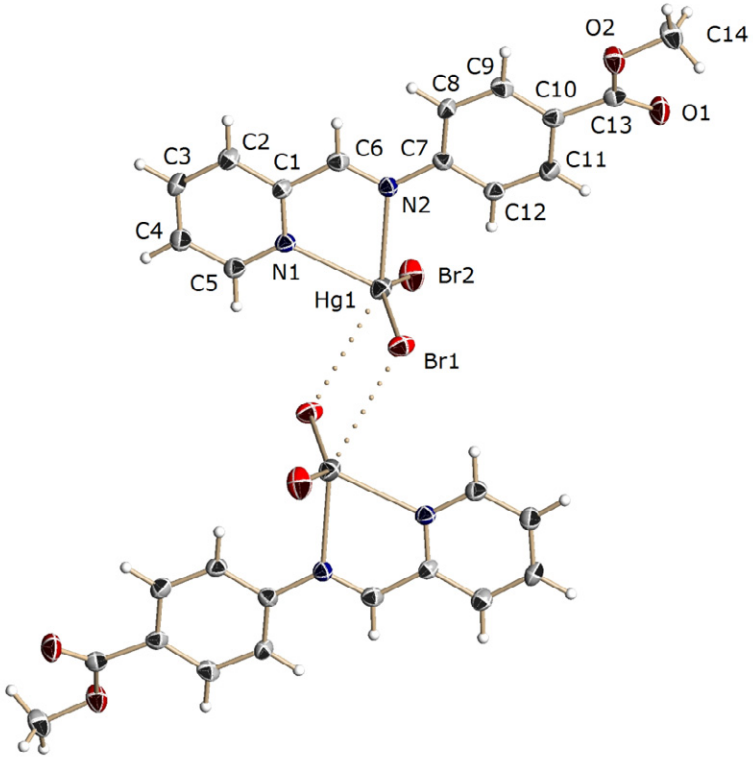

Fig. 7. Perspective view of binuclear $[HgBr_2L^5]_2$ **9a**. Displacement ellipsoids are drawn at the 50% probability level and unlabelled atoms are related by the symmetry operation 1-x, 1-y, 1-z.

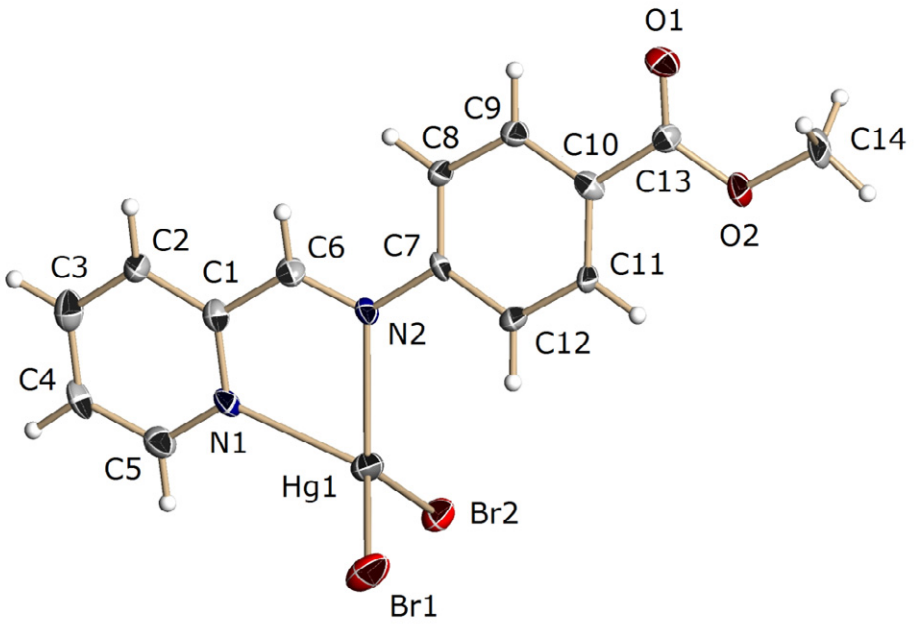

Fig. 8. Perspective view of mononuclear $[HgBr_2L^5]$ **9b**. Displacement ellipsoids are drawn at the 50% probability level.

In binuclear **9a** (Fig. 7), molecules aggregate about a centre of inversion *via* asymmetric μ_2-bromido bridges. In the unit cell of **9b** (Fig. 8), the molecules are orientated differently with the closest intermolecular Hg...Br contact being 4.3894(6) Å; further details are given below. The distance of the longer Hg–Br bond of the bridge in **9a**, *i.e.* 3.3759(5) Å, is marginally within the sum of the respective van der Waals radii, *i.e.* 3.40 Å, and this must be considered a weak interaction only [13]. However, the presence of the μ_2-bromido bridge in **9a**, even if weak, does have an impact upon the geometric parameters about the mercury atom. Thus, compared with the Hg–N bond lengths in **8**, there has been a significant reduction in asymmetry in **9a** and this asymmetry is reduced even further when intermolecular Hg...Br interactions are absent as in **9b**. The differences in the shorter Hg–X bond lengths is also impacted upon by bridging. In **8**, Δ(Hg–Cl) is 0.15 Å. When weak bridging is present (**9a**), Δ(Hg–Br) is 0.04 Å, and when absent Δ(Hg–

Br) is 0.02 Å. The observed trends also apply to the isomorphous mononuclear HgI_2 analogue, $[HgI_2L^5]$ (**10**, Fig. 9). Marked differences are also noted in coordination geometries. In penta-coordinated **9a**, the value of τ is 0.17, indicating that in both **8** and **9a**, the coordination geometry approaches square pyramidal more so than in the other binuclear compounds reported herein. By contrast, the coordination geometries of **9b** and **10** are distorted tetrahedral with ranges of angles subtended at mercury being 71.24(13)°, for the chelate angle, to 121.52(9)° for N2-Hg-Br2 (**9b**), and 69.75(10)° to 127.047(10)° for I1-Hg-I2 (**10**).

Finally, a comment on the relative orientations of the ester substituents in **8**, **9a**, **9b** and **10** is apposite. Each ester group is twisted out of the of the pyridyl ring to which it is connected, as quantified by the values of the C9–C10–C13–O1 torsion angles of -13.9(5), 157.6(5), 12.6(7) and -8.8(6)°, respectively. A difference in polymorphic **9a** and **9b** is noted in that the carbonyl-O1 atom is *syn* to the chelate ring in **9a** but anti in **9b**; anti orientations are noted in **8** and **10**. No correlation between the orientation of the ester group and crystal packing was found.

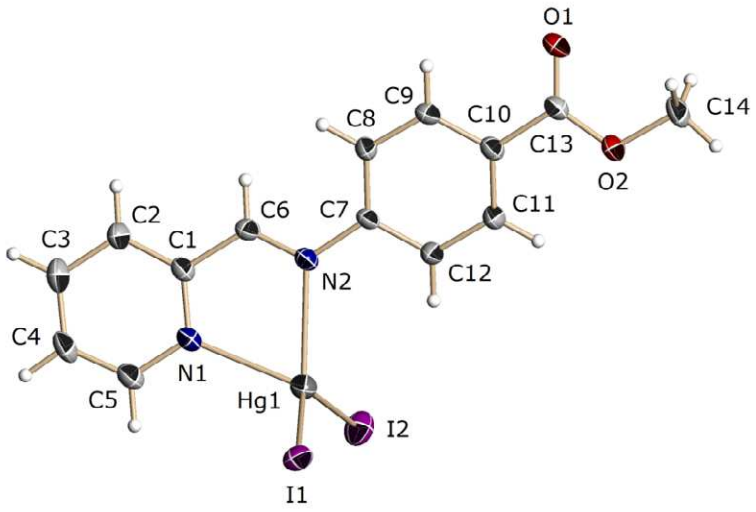

Fig. 9. Perspective view of mononuclear $[HgI_2L^5]$ **10**. Displacement ellipsoids are drawn at the 50% probability level.

One other full set of HgX_2, X = Cl, Br and I, structures, with an identical (*E*)-*N*-(pyridin-2-ylmethylidene)arylamine ligand has been reported, namely the 4-methyl derivatives, **1**-**3** (Scheme 1a; Table 3) [6]. The trend towards mononuclear structures observed for **8**-**10** is repeated in this series and was correlated with the increased electronegativity of the chlorido ligands which enhanced the capacity of the mercury atoms to expand their coordination spheres and thereby dimerize.

The final structure to be described is that of $[HgCl_2L^4]_2$ (**7**, Fig. 10). The L^4 ligand features a CO_2CH_3 ester residue in the 2-position of the aryl ring and while a binuclear structure arises owing to μ_2-chlorido bridges, as seen for the other $HgCl_2$ derivatives, a variation is observed in that the carbonyl-O1 forms a weak interaction Hg–O1 = 2.764(4) Å to the mercury atom. The presence of the coordinating O1 atom in **7** results in an increase in the Hg–N bond distances compared with those is the 4-substituted analogue, **8** (Table 3). The Hg...Cl1^i bridging distance is significantly longer in **7** than **8**, *i.e*. 3.2330(15) *cf*. 2.8929(7) Å, with the result that the Hg-Cl1 bond length is significantly reduced in **7**; symmetry operation i: -x, -y, -z. The Cl_3N_2O donor set approximates a distorted trigonal prism with the trigonal faces occupied by the (N1,Cl2,Cl1^i) and (N2,Cl1,O1) atoms.

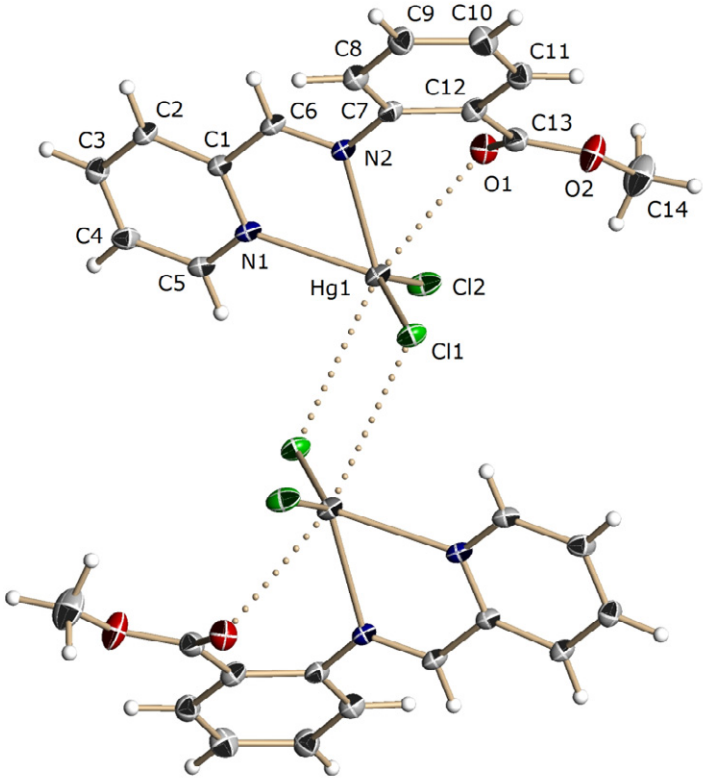

Fig. 10. Perspective view of binuclear $[HgCl_2L^4]_2$ **7**. Displacement ellipsoids are drawn at the 30% probability level and unlabelled atoms are related by the symmetry operation -x, -y, -z.

2.4. Supramolecular architectures

The crystal packing patterns in **4**-**10** are discussed in terms of common types. While no classical hydrogen bonding is observed, π...π interactions predominate. Sometimes the π-system is based on a chelate ring, which is known to have aromatic character [14,15]. These sorts of π...π interactions are increasingly being recognized as being important in the supramolecular chemistry of metal complexes [16-18]. Other interactions are often of the type, C–H...X and C–H...π, again, sometimes the chelate ring defines the π-system [18-20]. Analysis of the crystal packing is based on the standard geometric parameters embodied in PLATON [21]. Diagrams

were drawn with DIAMOND [22] and geometric parameters describing the intermolecular interactions are given in the respective figure captions.

The crystal packing of **4** is dominated by interactions occurring between π-systems. Columns of molecules parallel to the a-axis are stabilized by π(pyridyl)...π(arene) interactions, and these are connected into a three-dimensional architecture by C–H...π(chelate) interactions (Fig. 11). A similar pattern was observed in the crystal structure of **6** (Fig. S1). Here, molecules aligned along the a-axis are connected by π(pyridyl)...π(arene) interactions as for **4**, but in this case the columns are connected by additional π(arene)...π(arene) interactions as well as C–H...Cl contacts; the Cl2 atom is bifurcated.

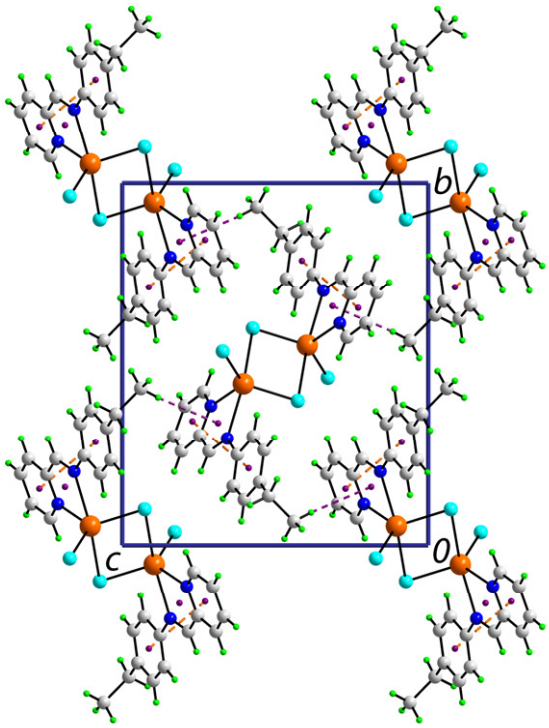

Fig. 11. View in projection down the a-axis of the unit cell contents of $[HgCl_2L^1]_2$ **4**. The C–H...π(chelate) [C14–H14c...Cg(HgN_2C_2)^i = 2.82 Å, C14...Cg(HgN_2C_2)^i = 3.743(14) Å, angle at H14c = 162° for symmetry operation i: ½+x, ½-y, -½+z] and π...π [Cg(N1,C1-C5)...Cg(C7-

C12)^{ii} = 3.834(5) Å, angle of inclination = 10.8(4)° for ii: -1+x, y, z] interactions are shown as purple and orange dashed lines, respectively.

In **5**, a different pattern is observed, based on supramolecular layers of molecules parallel to (-4 1 0). These form as a result of C–H...O, C–H...Cl (H…Cl = 2.75 Å) and π(pyridyl)...π(arene) interactions. The stacked layers are connected by π(arene)...π(arene), C–H...π(chelate) and C–H...Cl interactions (Fig. 12). Analogous layers of molecules stack along the b-axis in the crystal structure of **8** (Fig. S2) with the primary connections between them being of the type π(pyridyl)...π(arene).

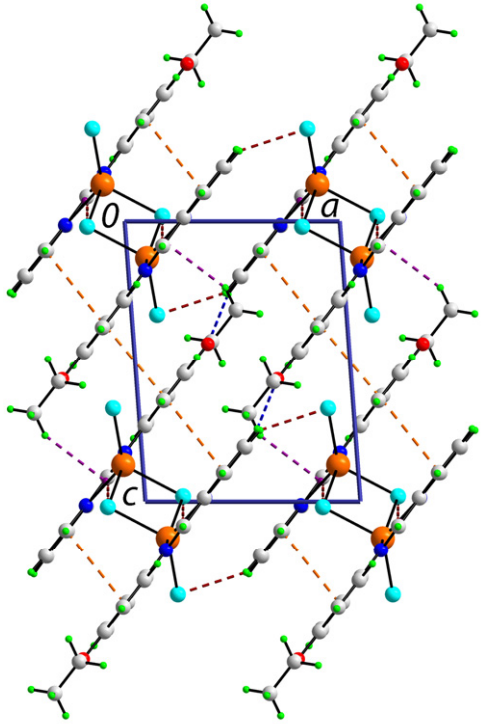

Fig. 12. View in projection down the b-axis of the unit cell contents of $[HgCl_2L^2]_2$ **5**. The C–H...π(chelate) [C14–H143...Cg(HgN_2C_2)^{i} = 2.81 Å, C14...Cg(HgN_2C_2)^{i} = 3.652(5) Å, angle at H143 = 144° for symmetry operation i: -x, 1-y, 1-z], π...π [Cg(N1,C1-C5)...Cg(C7-C12)^{ii} = 3.636(2) Å, angle of inclination = 1.3(2)° for ii: -x, 1-y, -z; Cg(C7-C12)...Cg(C7-C12)^{iii} =

3.599(2) Å, for iii: -x, 1-y, 1-z], C–H...O [C3–H3...O1^{iv} = 2.53 Å, C3...O1^{iv} = 3.457(5) Å, angle at H3 = 167° for iv: 1+x, y, -1+z] and C–H...Cl [C4–H4...Cl2^{v} = 2.77 Å, C4...Cl2^{v} = 3.616(5) Å, angle at H4 = 169° for v: 1-x, -y, -z; C6–H6...Cl1^{ii} = 2.75 Å, C4...Cl2^{v} = 3.639(4) Å, angle at H6 = 155°] interactions are shown as purple, orange, blue and brown dashed lines, respectively.

In polymorph **9a**, the layers are parallel to (1 1 0) and are stabilized as a result of C–H...O, C–H...Br (H…Br = 3.05 Å) and π(pyridyl)...π(arene) interactions. The stacked layers are connected by π(arene)...π(arene), C–H...π(chelate) and additional C–H...Br interactions (Fig. 13).

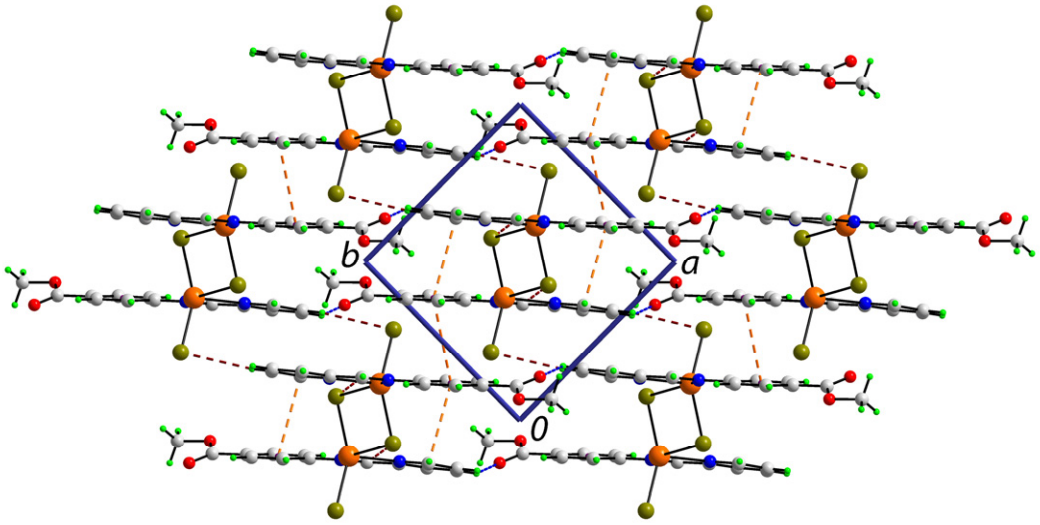

Fig. 13. View in projection down the c-axis of the unit cell contents of $[HgBr_2L^5]_2$ **9a**. The π...π [Cg(N1,C1-C5)...Cg(C7-C12)^{i} = 3.705(3) Å, angle of inclination = 9.0(2)° for i: 1-x, 1-y, -z; Cg(C7-C12)...Cg(C7-C12)^{ii} = 3.706(3) Å, for ii: -x, 1-y, -z], C–H...O [C3–H3...O1^{iii} = 2.32 Å, C3...O1^{iii} = 3.119(6) Å, angle at H3 = 142° for iii: 1+x, -1+y, z] and C−H...Br interactions [C4–H4...Br2^{iv} = 3.04 Å, C4...Br2^{iv} = 3.936(5)Å, angle at H4 = 157° for iv: 1-x, -y, 1-z; C6–H6...Br1^{i} = 3.05 Å, C6...Br1^{i} = 3.903(4)Å, angle at H6 = 150°] interactions are shown as orange, blue and brown dashed lines, respectively.

In **9b**, supramolecular chains along the a-axis are formed as a result of π(pyridyl)...π(arene) as well as π(chelate)...π(arene) interactions along with C–H...Br contacts (Fig. 14a). These are connected into layers by rather strong C–H...O contacts. The layers stack along the b-axis without specific interactions between them (Fig. 14b). The crystal structure of **10** is isomorphous with **9b** and full details are given in the Supplementary Materials (Fig. S3).

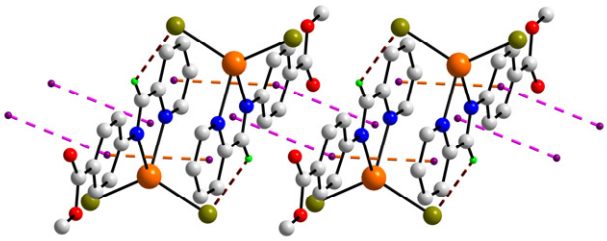

(a)

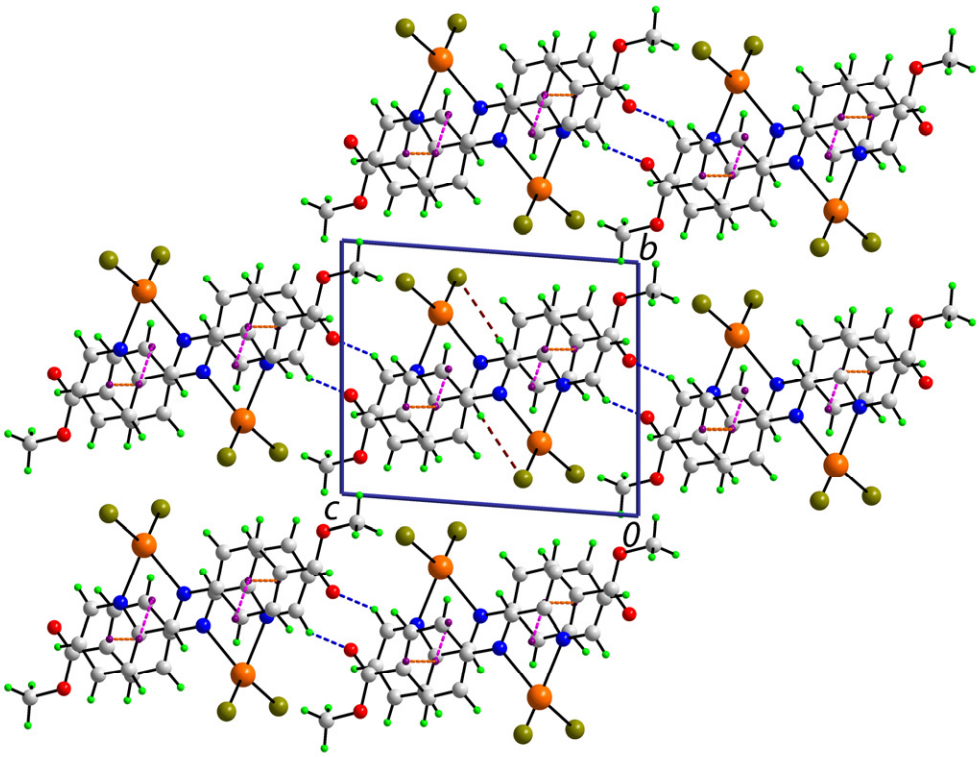

(b)

Fig. 14 (a) View of the supramolecular chain aligned along the a-axis in $[HgBr_2L^5]_2$ **9a**. (b) View in projection down the a-axis of the unit cell contents, highlighting the stacking of layers along the b-axis. The π...π [Cg(N1,C1-C5)...Cg(C7-C12)^{i} = 3.687(3) Å, angle of inclination = 9.7(2)° for i: 1-x, 1-y, 1-z; Cg(HgN_2C_2)...Cg(C7-C12)^{ii} = 3.880(3) Å, angle = 9.2(2)° for ii: -x, 1-y, -z], C−H...O [C5–H5...O1^{iii} = 2.28 Å, C5...O1^{iii} = 3.083(7) Å, angle at H5 = 142° for iii: 1+x, y, -1+z] and C−H...Br interactions [C6–H6...Br2^{i} = 2.91 Å, C6...Br2^{i} = 3.632(5)Å, angle at H6 = 134°] interactions are shown as orange (pink for chelate ring), blue and brown dashed lines, respectively.

The polymorphic structures of **9a** and **9b** have clearly distinguishable patterns of packing with the stark difference relating to the relative orientations of the $HgBr_2$ fragments. In **9a**, where these approach each other *via* Hg...Br interactions, the packing index computes to 74.0%. A significantly less efficient packing index of 68.5% is found for **9b**, suggesting that 9a is thermodynamically more stable.

Finally, the molecules in the crystal structure of $[HgCl_2L^4]_2$ **7** are linked into layers in the bc-plane by π(chelate)...π(arene) and C–H...O contacts (Fig. 15a) and consolidated into a three-dimensional architecture by C–H...Br contacts (Fig. 15b).

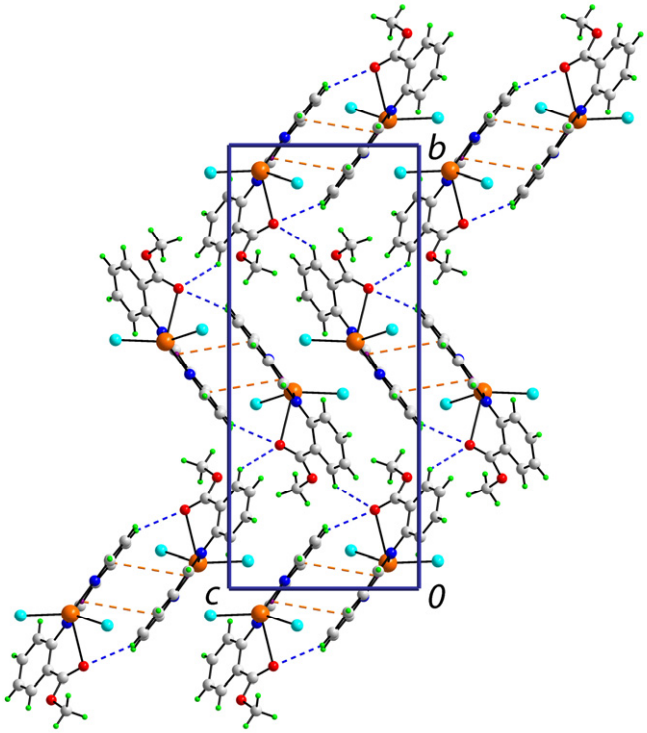

370

371 (a)

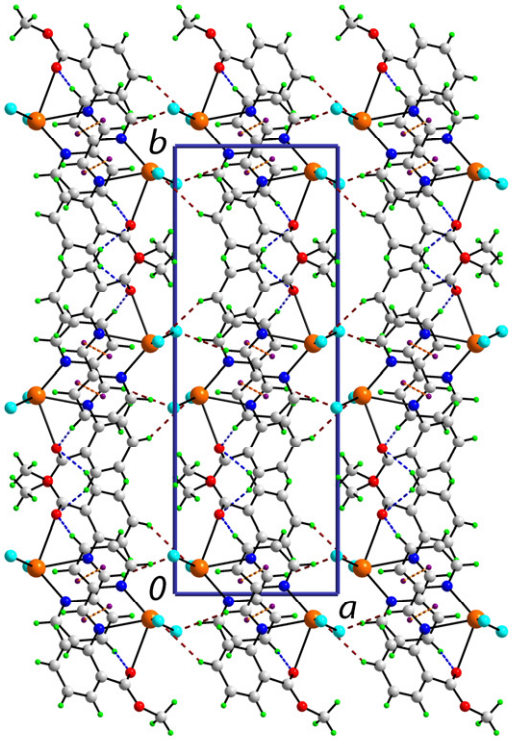

372

373 (b)

Fig. 15. (a) View of the supramolecular layer in $[HgCl_2L^4]_2$ **7**. (b) View in projection down the a-axis of the unit cell contents, highlighting the stacking of layers along the a-axis and the C–H...Cl connections between them. The π...π [Cg(HgN_2C_2)...Cg(C7-C12)^{i} = 3.821(3) Å, angle of inclination = 3.2(2)° for i: 1-x, -y, 1-z], C–H...O [C3–H3...O1^{i} = 2.60 Å, C3...O1^{i} = 3.418(7) Å, angle at H3 = 146°; C11–H11...O1^{ii} = 2.54 Å, C11...O1^{ii} = 3.291(8) Å, angle at H3 = 136° for ii: x, ½-y, -½+z] and C–H...Cl [C6–H6...Cl2^{iii} = 2.73 Å, C6...Cl2^{iii} = 3.559(6) Å, angle at H5 = 146° for iii: 1+x, y, z; C9–H9...Cl1^{iii} = 2.81 Å, C9...Cl1^{iii} = 3.558(7) Å, angle at H5 = 136°] interactions are shown as orange, blue and brown dashed lines, respectively.

3. Conclusion

On the basis of the newly described structures and those of literature precedents, the preponderance of binuclear structures observed when $HgCl_2$ is complexed with (*E*)-*N*-(pyridin-2-ylmethylidene)arylamine ligands is not repeated in the $HgBr_2$ and HgI_2 analogues, an observation correlated with the enhanced Lewis acidity of the mercury centres when X = Cl. Within the series of $HgCl_2$ compounds with (*E*)-*N*-(pyridin-2-ylmethylidene)-4-substituted-phenylamines, asymmetry in the mode of coordination of the chelate could be moderated by increasing the electronegativity of the substituent, owing to the weakening of the Hg-N(imino) bond.

4. Experimental

4.1. General considerations

Caution! *Compounds of mercury are highly toxic* [23]. *Care must be taken when handling samples, and appropriate disposal procedures are necessary.* All chemicals were used as purchased without purification: $HgCl_2$, pyridine-2-carboxaldehyde (Merck), $HgBr_2$, HgI_2 (Fine

Chemicals), *p*-ethylaniline (Aldrich), *p*-ethoxylaniline (Across), *p*-chloroaniline, methylanthranilate, *p*-aminobenzoic acid (Hi-Media). Methyl *p*-aminobenzoate was prepared by reacting *p*-aminobenzoic acid and $SOCl_2$ in methanol by literature method [24]. The (*E*)-N-(pyridin-2-ylmethylidene)arylamine derivatives L^1-L^5 were prepared *in situ* from pyridine-2-carboxaldehyde and the corresponding aniline. Solvents were purified by standard procedures and were freshly distilled prior to use. Elemental analyses, solution electrical conductivity measurements, IR, ^{1}H NMR and Uv-Vis spectra were recorded on instruments and under conditions as described elsewhere [6]. Fluorescence spectra were obtained on a Hitachi model FL4500 spectrofluorimeter (with the excitation and emission slits fixed at 10 and 20 nm, respectively) and all spectra were corrected for the instrument response function and conditions as described earlier [6].

*4.2. Synthesis of mercury compounds (**4**-**10**)*

The preparations of the dihalomercury(II) compounds **4**-**10** are very similar, so that the preparation of the dichloride derivative **4** is given here as a representative case.

4.2.1. $[HgCl_2L^1]_2$ (**4**). To a solution of pyridine-2-carboxaldehyde (0.13 g, 1.23 mmol) in ethanol (3 ml) was added a solution of *p*-ethylaniline (0.15 g, 1.23 mmol) in ethanol (2 ml). The mixture was stirred at ambient temperature for 30 min. To this reaction mixture, a solution of $HgCl_2$ (0.33 g, 1.22 mmol) in methanol (20 ml) was added drop-wise under stirring conditions which resulted in the immediate formation of a yellow precipitate. The stirring was continued for 3 h and then the mixture was filtered. The residue was washed with methanol (3 x 5 ml) and dried *in vacuo*. The dried solid was dissolved by boiling in 40 ml of acetonitrile and filtered while hot. The filtrate, upon cooling to r.t., afforded yellow crystalline material. Yield 0.29 g

(47%). M.p. 213-215 °C. Found: C, 34.80; H, 3.12; N, 5.80%. Calc. for $C_{28}H_{28}Cl_4Hg_2N_4$: C, 34.88; H, 2.93; N, 5.82%. Λ_m (CH_3CN): 6 $\Omega^{-1}cm^2mol^{-1}$. IR (cm^{-1}): 1622 ν_{asym}(C(H)=N); 1592, 1485, 1439 ν(C=N)py. ^{1}H NMR (DMSO-d_6): 8.93 [s, 1H, H-7], 8.55 [d, *J* = 4.0 Hz, 1H, H-3'], 8.11 [t, *J* = 8.0 Hz, 1H, H-6'], 8.02 [d, *J* = 8.0 Hz, 1H, H-5'], 7.72 [t, *J* = 6.4 Hz, 1H, H-4'], 7.53 [d, *J* = 8.0 Hz, 2H, H-3,5], 7.31 [d, *J* = 8.0 Hz, 2H, H-2,6], 2.67 [q, 2H, CH_2], 1.26 [t, 3H, CH_3] ppm.

Compounds **5**-**10** were prepared as yellow crystals in a manner similar to that described for the preparation of **4**, using appropriate anilines and mercury(II) halides as a starting materials.

4.2.2. [$HgCl_2L^2$]$_2$ (**5**). A similar synthetic procedure as for **4** was used except that *p*-ethylaniline was replaced by *p*-ethoxylaniline, giving pale yellow crystals from acetonitrile solution. Yield 46%. M.p. 194-195 °C. Found: C, 33.85; H, 2.99; N, 5.80%. Calc. for $C_{28}H_{28}Cl_4Hg_2N_4O_2$: C, 33.76; H, 2.84; N, 5.63%. Λ_m (CH_3CN): 6 $\Omega^{-1}cm^2mol^{-1}$. IR (cm^{-1}): 1623 ν_{asym}(C(H)=N); 1588, 1476, 1445 ν(C=N)py. ^{1}H NMR (DMSO-d_6): 8.97 [s, 1H, H-7], 8.88 [d, *J* = 4.0 Hz, 1H, H-3'], 8.10 [m, 2H, H-5',6'], 7.70 [t, br, 1H, H-4'], 7.59 [d, *J* = 8.0 Hz, 2H, H-3,5], 6.68 [d, *J* = 8.0 Hz, 2H, H-2,6], 4.08 [q, 2H, CH_2], 1.42 [t, 3H, CH_3] ppm.

4.2.3. [$HgCl_2L^3$]$_2$ (**6**). A similar synthetic procedure as for **4** was used except that *p*-ethylaniline was replaced by *p*-chloroaniline, giving pale yellow crystals from acetonitrile solution. Yield 40%. M.p. 243-245 °C. Found: C, 29.60; H, 1.68; N, 5.79%. Calc. for $C_{24}H_{18}Cl_6Hg_2N_4$: C, 29.51; H, 1.86; N, 5.74%. Λ_m (CH_3CN): 8 $\Omega^{-1}cm^2mol^{-1}$. IR (cm^{-1}): 1618 ν_{asym}(C(H)=N); 1589, 1482, 1436 ν(C=N)py. ^{1}H NMR (DMSO-d_6): 8.89 [d, *J* = 4.0 Hz, 1H, H-3'], 8.87 [s, 1H, H-7],

8.10 [m, 2H, H-5',6'], 7.70 [t, br, 1H, H-4'], 7.50 [d, *J* = 8.0 Hz, 2H, H-3,5], 7.44 [d, *J* = 8.0 Hz, 2H, H-2,6] ppm.

4.2.4. $[HgCl_2L^4]_2$ (**7**). A similar synthetic procedure as for **4** was used except that *p*-ethylaniline was replaced by methylanthranilate and reaction was conducted under ice-cold conditions, giving pale yellow single crystals from acetonitrile solution. Yield 50%. M.p.158-160 °C. Found: C, 33.85; H, 2.42; N, 5.57%. Calc. for $C_{28}H_{24}Cl_4Hg_2N_4O_4$: C, 32.84; H, 2.36; N, 5.47%. Λ_m (CH_3CN): 8 $\Omega^{-1}cm^2mol^{-1}$. IR (cm^{-1}): 1700 ν_{asym}(OCO), 1620 ν_{asym}(C(H)=N); 1592, 1485, 1438 ν(C=N)py. ^{1}H NMR (DMSO-d_6): 10.14 [s, 1H, H-7], 8.83 [d, *J* = 4.0 Hz, 1H, H-3'], 7.95 [m, 2H, H-3,4], 7.83 [d, *J* = 8.0 Hz, 1H, H-6'], 7.60 [t, *J* = 8.0 Hz, 1H, H-5'], 7.26 [t, *J* = 6.4 Hz, 1H, H-5], 6.70 [d, *J* = 6.4 Hz, 1H, H-6], 6.62 [t, *J* = 6.4 Hz, 1H, H-4'], 3.86 [s, 3H, $OCOCH_3$] ppm.

4.2.5. $[HgCl_2L^5]_2$ (**8**). A similar synthetic procedure as for **4** was used except that *p*-ethylaniline was replaced by methyl *p*-aminobenzoate, giving pale yellow crystals from acetonitrile solution. Yield 50%. M.p. 208-210 °C. Found: C, 33.05; H, 2.52; N, 5.86%. Calc. for $C_{28}H_{24}Cl_4Hg_2N_4O_4$: C, 32.84; H, 2.36; N, 5.47%. Λ_m (CH_3CN): 6 $\Omega^{-1}cm^2mol^{-1}$. IR (cm^{-1}): 1712 ν_{asym}(OCO), 1622 ν_{asym}(C(H)=N); 1593, 1427 ν(C=N)py. ^{1}H NMR (DMSO-d_6): 8.92 [d, *J* = 4.0 Hz, 1H, H-3'], 8.90 [s, 1H, H-7], 8.13 [t, *J* = 8.0 Hz, 1H, H-6'], 8.05 [d, *J* = 8.0 Hz, 1H, H-5'], 7.80 [t, *J* = 6.4 Hz, 1H, H-4'], 7.59 [d, 2H, *J* = 8.0 Hz, H-3,5], 6.64 [d, 2H, *J* = 8.0 Hz, H-2,6], 3.94 [s, 3H, CO_2CH_3] ppm.

4.2.6. $HgBr_2L^5$ (**9**). A similar synthetic procedure as for **4** was used except that $HgCl_2$ and *p*-ethylaniline were replaced by $HgBr_2$ and methyl *p*-aminobenzoate, giving pale yellow crystals. Yield 52%. Crystals of compound $[HgBr_2L^5]_2$: **9a** and $HgBr_2L^5$: **9b** (both prism type, gave

similar microanalytical and spectroscopic data and were indistinguishable) were obtained from acetonitrile from two different batches of samples (see X-ray discussion for structural details). M.p.: **9a** 218-220 °C; **9b** 143-145 °C. Found: C, 28.50; H, 2.10; N, 4.80%. Calc. for $C_{28}H_{24}Br_4Hg_2N_4O_4$: C, 27.98; H, 2.01; N, 4.66%. Λ_m (CH_3CN): 6 $\Omega^{-1}cm^2mol^{-1}$. IR (cm^{-1}): 1712 ν_{asym}(OCO), 1646 ν_{asym}(C(H)=N); 1593, 1434 ν(C=N)py. ^{1}H NMR (DMSO-d_6): 9.02 [s, 1H, H-7], 8.89 [d, J = 4.0 Hz, 1H, H-3'], 8.15 [m, 4H, H-5',6',3,5], 7.79 [t, J = 6.4 Hz, 1H, H-4'], 7.61 [d, J = 8.0 Hz, 2H, H-2,6], 3.94 [s, 3H, CO_2CH_3] ppm.

4.2.7. $[HgI_2L^5]_2$ (**10**): A similar synthetic procedure as for **4** was used except that $HgCl_2$ and *p*-ethylaniline were replaced by HgI_2 and methyl *p*-aminobenzoate, giving pale yellow crystals. Yield 49%. M.p. 198-200 °C. Found: C, 24.40; H, 1.52; N, 4.17%. Calc. for $C_{14}H_{12}I_2HgN_2O_2$: C, 24.19; H, 1.74; N, 4.03%. Λ_m(CH_3CN): 7 $\Omega^{-1}cm^2mol^{-1}$. IR (cm^{-1}):1712 ν_{asym}(OCO), 1639 ν_{asym}(C(H)=N); 1553, 1434 ν(C=N)py. ^{1}H-NMR (DMSO-d_6): 9.11 [s, 1H, H-7], 8.81 [d, J = 4.0 Hz, 1H, H-3'], 8.18 [t, br, 1H, H-6'], 8.13 [d, J = 8.0 Hz, 2H, H-3,5], 7.96 [d, br, 1H, H-5'], 7.80 [t, br, 1H, H-4'], 7.65 [d, J = 8.0 Hz, 2H, H-2,6], 3.93 [s, 3H, CO_2CH_3] ppm.

4.3. X-ray data collection and structure determinations

Crystals of compounds suitable for an X-ray crystal-structure determination were obtained from acetonitrile (**4**, **6**, **9a**, **9b** and **10**), acetonitrile/acetone (**7**) and acetonitrile/methanol (**5** and **8**) by slow evaporation of the solvent at room temperature. In the case of compound **9**, two crystalline polymorphs (**9a** and **9b**) were isolated from two different batches of crystals obtained from acetonitrile solution. The measurements for **5**, **7** and **10** were made at low temperature on a Nonius KappaCCD diffractometer [25] with graphite-monochromated Mo Kα radiation (λ = 0.71073 Å) and an Oxford Cryosystems Cryostream 700 cooler. The data for **8**, **9a** and **9b** were

recorded on an Agilent Technologies SuperNova area-detector diffractometer [26] using Mo Kα radiation from a micro-focus X-ray source and an *Oxford Instruments Cryojet XL* cooler, while the data for **4** and **6** were recorded on a Bruker-APEX diffractometer equipped with a CCD area detector and Mo Kα radiation. Data reduction on **5**, **7** and **10** was performed with HKL Denzo and Scalepack [27], with CrysAlisPro [26] for **8**, **9a** and **9b**, and with SAINT [28] for **4** and **6**. The intensities were corrected for *Lorentz* and polarization effects. An empirical absorption correction based on the multi-scan method [29,30] using spherical harmonics was applied for **4**-**8**, an analytical absorption correction [31] was applied for **9a** and **9b** and a numerical absorption correction [32] was applied for **10**. Equivalent reflections were merged. The structures of compounds **5**, **7** and **10** were solved by heavy-atom Patterson methods [33], which initially revealed the position of the mercury atom, while all remaining non-hydrogen atoms were located in a Fourier expansion of the Patterson solution, which was performed by *DIRDIF94* [34]. The structures of **4**, **6**, **8**, **9a** and **9b** were solved by direct methods using *SHELXS97* [35], which revealed the positions of all non-hydrogen atoms. The non-hydrogen atoms in each structure were refined anisotropically. All of the H-atoms were placed in geometrically calculated positions and refined by using a riding model where each H-atom was assigned an isotropic displacement parameter with a value equal to $1.2U_{eq}$ of its parent atom ($1.5U_{eq}$ for methyl-H). The refinement of each structure was carried out on F^2 by using full-matrix least-squares procedures, which minimized the function $\Sigma w(F_o^2–F_c^2)^2$. A correction for secondary extinction was applied for **5**, **8**, **9a**, **9b** and **10**. One reflection in **5** and **8**, and six reflections in **9b** and **10** were omitted owing to poor agreement. The binuclear molecules within the crystal structures of **4**-**7**, **8** and **9a** are located across crystallographic inversion centers. In the case of **4**, the enlarged atomic displacement parameters of the ethyl C atoms suggest the group might be

518 conformationally disordered. A disorder model was not developed, but bond length restraints of
519 1.500(5) and 1.540(5) Å were applied to the ring-methylene and methylene-methyl C–C bonds,
520 respectively, of the ethyl group. Several data sets exhibited some elevated residual electron
521 density peaks, which is not an uncommon observation with heavy-atom structures. These
522 residual peaks were generally located within 1.2 Å of the heaviest atoms in the structure (Hg, Br
523 or I), but in the cases of **5** and **8**, they were located in chemically meaningless positions. The
524 largest residual peaks found for **7**, 4.54 and 4.06 e $Å^{-3}$, were symmetrically disposed within 0.8 Å
525 of the Hg atom and the next highest peak was 1.37 e $Å^{-3}$. Trials with various absorption
526 corrections did not change the results. No evidence for twinning or disorder was found. The
527 *SHELXTL-NT* program package [35] was used for the refinement of **4** and **6**, while *SHELXL97*
528 [36] was used for the refinement of the other structures. The data collection and refinement
529 parameters are given in Table 2, and perspective views of the molecular structures, generated
530 with *SHELXTL-NT* [35], are shown in Figs. 3-10.
531
532 **Appendix A. Supplementary material**
533 CCDC-915973 (for **10**), -915974 (for **4**), -915975 (for **5**), -915976 (for **6**), -915977 (for **7**), -
534 915978 (for **8**), -915979 (for **9a**) and -915980 (for **9b**) contain the supplementary
535 crystallographic data for this paper. These data can be obtained free of charge from The
536 Cambridge Crystallographic Data Centre *via* www.ccdc.cam.ac.uk/data_request/cif.
537 Supplementary data (Fig. S1: View in projection down the a-axis of the unit cell contents of
538 $[HgCl_2L^3]_2$ **6**. Fig. S2: View in projection down the c-axis of the unit cell contents of $[HgCl_2L^4]_2$
539 **8**. Fig. S3: View in projection down the a-axis of the unit cell contents of $[HgI_2L^5]_2$ **10**,

highlighting the stacking of layers along the b-axis) associated with this article can be found in the online version, at http://XXXX

Acknowledgments

The financial support of the Department of Science & Technology, New Delhi, India (Grant No.SR/S1/IC-03/2005,TSBB), the University Grants Commission, New Delhi, India through SAP-DSA, Phase-III and Indo-Swiss Joint Research Programme, Joint Utilisation of Advanced Facilities (Grant No. JUAF 11, TSBB, AL) are gratefully acknowledged. Support from the Ministry of Higher Education, Malaysia, High-Impact Research scheme (UM.C/HIR-MOHE/SC/03) is also gratefully acknowledged.

572 **References**
573

574 [1] N. N. Greenwood, A. Hughes, M. Fox, K. Dillon, K. Wade, Chemistry of Elements, 3rd
575 edition, Elsevier, 2011.
576 [2] R. J. Baker, C. Jones, Dalton Trans. (2005) 1341-1348.
577 [3] G. Bouhadir, D. Bourissou, Chem. Soc. Rev. 33 (2004) 210-217.
578 [4] D. Braga, G. R. Desiraju, J. S. Miller, A. G. Orpen, S. L. Price, CrystEngComm. 4 (2002)
579 500-509.
580 [5] G. R. Desiraju, Chem. Commun. (1997) 1475-1482.
581 [6] T. S. Basu Baul, S. Kundu, S. Mitra, H. Höpfl, E. R. T. Tiekink, A. Linden, Dalton Trans. 42
582 (2013) 1905-1920.
583 [7] C. Silvestru, I. Haiduc, Coord. Chem. Rev. 147 (1996) 117-146.
584 [8] E. R. T. Tiekink, Main Group Chemistry News 3 (1995) 12-16.
585 [9] M. J. Cox, E. R. T. Tiekink, Rev. Inorg. Chem. 17 (1997) 1-23.
586 [10] K. Nakamoto, Infrared and Raman Spectra of Inorganic and Coordination Compounds,
587 Wiley, New York, 1986.
588 [11] G. Mahmoudi, A. Morsali, Polyhedron 27 (2008) 1070-1078.
589 [12] A. W. Addison, T. N. Rao, J. Reedijk, J. van Rijn, G. C. Verschoor, J. Chem. Soc., Dalton
590 Trans. (1984) 1349-1356.
591 [13] A. Bondi, J. Phys. Chem. 68 (1964) 441-452.
592 [14] H. Masui, Coord. Chem. Rev. 219-221 (2001) 957-992.
593 [15] Y. Z. Wang, G. H. Robinson, Organometallics 26 (2007) 2-11.
594 [16] Z. D. Tomić, D. N. Sredojević, S. D. Zarić, Cryst. Growth Des. 6 (2006) 29-31.
595 [17] D. N. Sredojević, Z. D. Tomić, S. D. Zarić, Cryst. Growth Des. 10 (2010) 3901-3908.

596 [18] E. R. T. Tiekink, in Crystal Engineering. Supramolecular Chemistry: from Molecules to
597 Nanomaterials (Eds.: J. W. Steed, P.A. Gale), John Wiley & Sons Ltd, Chichester, UK,
598 2012, pp. 2791-2828.
599 [19] M. K. Milčič, V. B. Medaković, D. N. Sredojević, N. O. Juranić, S. D. Zarić, Inorg. Chem.
600 45 (2006) 4755-4763.
601 [20] E. R. T. Tiekink, J. Zukerman-Schpector, Chem. Commun. 47 (2011) 6623-6625.
602 [21] A. L. Spek, Acta Crystallogr. Sect. D 65 (2009) 148-155.
603 [22] K. Brandenburg, DIAMOND. Crystal Impact GbR, Bonn, Germany, 2006
604 [23] A. J. Bloodworth, J. Organomet. Chem. 23 (1970) 27-30.
605 [24] T. S. Basu Baul, S. Basu, E. R. T. Tiekink, Acta Crystallogr. Sect. E 63 (2007) o3358.
606 [25] R. Hooft, KappaCCD Collect Software, Nonius BV, Delft, The Netherlands, 1999.
607 [26] CrysAlisPro, Version 1.171.33.55, Agilent Technologies, Yarnton, Oxfordshire, England,
608 2010.
609 [27] Z. Otwinowski, W. Minor, in Methods in Enzymology, (Eds.: C.W. Carter Jr., R. M. Sweet),
610 vol. 276, Macromolecular Crystallography, Part A, Academic Press, New York, 1997, pp.
611 307-326.
612 [28] Bruker Analytical X-ray Systems, SAINT-NT Version 6.04, 2001.
613 [29] R. H. Blessing, Acta Crystallogr. Sect. A 51 (1995) 33-38.
614 [30] CrysAlisPro, Version 1.171.33.66, Agilent Technologies, Yarnton, Oxfordshire, England,
615 2010.
616 [31] R. C. Clark, J. S. Reid, Acta Crystallogr. Sect. A 51 (1995) 887-897.
617 [32] P. Coppens, L. Leiserowitz, D. Rabinovich, Acta Crystallogr. 18 (1965) 1035-1038.

[33] P. T. Beurskens, G. Admiraal, G. Beurskens, W. P. Bosman, S. Garcia-Granda, R. O. Gould, J. M. M. Smits, C. Smykalla, PATTY: The DIRDIF Program System, Technical Report of the Crystallography Laboratory, University of Nijmegen, The Netherlands, 1992.

[34] P. T. Beurskens, G. Admiraal, G. Beurskens, W. P. Bosman, R. de Gelder, R. Israel, J. M. M. Smits, DIRDIF94: The DIRDIF Program System, Technical Report of the Crystallography Laboratory, University of Nijmegen, The Netherlands, 1994.

[35] Bruker Analytical X-ray Systems, SHELXTL-NT Version 6.10, 2000.

[36] G. M. Sheldrick, Acta Crystallogr. Sect. A, 64 (2008) 112-122.

659 **Table 1**

660 Photophysical data for compounds **1**-**10** in acetonitrile solution[a]

Compounds	Electronic spectroscopic data λ_{max} (nm); (ε[M^{-1} cm^{-1}])	Photoluminescence data λ_{em}(nm)[c]	ϕ_F
1	348 (10781)	413, 429	0.16
2	341 (13367)	410, 432	0.20
3	340 (32679)	411, 433	0.02
4	344 (32273)	414, 427	0.13
5	352 (50678)	416, 428	0.19
6	348 (22206)	414, 428	0.18
7	338 (49032)	395	0.24
8	332 (28931)	414, 430	0.14
9a[b]	323 (28506)	418, 429	0.16
10	340 (20780)	412, 429	0.18

661 [a] Data for the compounds **1**-**3** (Scheme **1a**) were taken from ref. 6.

662 [b] Identical photophysical results were obtained for **9b**.

663 [c] The long wavelength emission appears as a shoulder in all cases except in **7**.

664
665
666
667
668
669
670
671
672
673
674
675
676
677

678
679 **Table 2**

680 Crystal data, data collection and refinement parameters for compounds **4**-**10**.

	4	**5**	**6**	**7**
Empirical formula	$C_{28}H_{28}Cl_4Hg_2N_4$	$C_{28}H_{28}Cl_4Hg_2N_4O_2$	$C_{24}H_{18}Cl_6Hg_2N_4$	$C_{28}H_{24}Cl_4Hg_2N_4O_4$
Formula weight	963.52	995.37	976.30	1023.33
Crystal size [mm]	$0.16 \times 0.19 \times 0.24$	$0.10 \times 0.15 \times 0.23$	$0.08 \times 0.16 \times 0.20$	$0.15 \times 0.23 \times 0.35$
Crystal morphology	Block	Tablet	Block	Tablet
Temperature [K]	293(2)	160(1)	100(2)	160(1)
Crystal system	Monoclinic	Triclinic	Monoclinic	Monoclinic
Space group	$P2_1/n$	$P\bar{1}$	$P2_1/n$	$P2_1/c$
a [Å]	7.9022(10)	8.0668(2)	7.5555(7)	7.8632(1)
b [Å]	15.1805(19)	9.0951(2)	15.1188(14)	21.4478(5)
c [Å]	12.8797(16)	10.5354(2)	12.1988(12)	9.2592(1)
α[°]	90	80.9248(13)	90	90
β[°]	95.907(2)	84.2979(11)	95.323(2)	98.5421(11)
γ[°]	90	79.8835(14)	90	90
V [Å^3]	1536.8(3)	749.38(3)	1387.5(2)	1544.23(4)
Z	2	1	2	2
D_x [g cm^{-3}]	2.082	2.205	2.337	2.201
μ [mm^{-1}]	10.350	10.643	11.652	10.338
Transmission factors [min, max]	0.19, 0.29	0.17, 0.39	0.20, 0.46	0.10, 0.24
θ range[°]	2–25	2–30	2–25	2–30
Reflections measured	14471	22765	13015	36430
Independent reflections; R_{int}	2707; 0.045	4348; 0.073	2436; 0.051	4494; 0.089
Reflections with $I > 2\sigma(I)$	2291	3884	2246	3979
Number of parameters	173	183	163	191
$R(F)$ [$I > 2\sigma(I)$reflns]	0.037	0.033	0.036	0.046
$wR(F^2)$ [all data]	0.084	0.087	0.068	0.138
GOF(F^2)	1.060	1.045	1.211	1.099
$\Delta\rho_{max, min}$ [e Å^{-3}]	1.50, -0.51	1.98, -2.85	1.26, -1.54	4.54, -3.41

681
682 Table 2 contd....

	8	**9a**	**9b**	**10**
Empirical formula	$C_{28}H_{24}Cl_4Hg_2N_4O_4$	$C_{28}H_{24}Br_4Hg_2N_4O_4$	$C_{14}H_{12}Br_2HgN_2O_2$	$C_{14}H_{12}HgI_2N_2O_2$
Formula weight	1023.33	1201.14	600.57	694.57
Crystal size [mm]	$0.10 \times 0.20 \times 0.38$	$0.10 \times 0.20 \times 0.30$	$0.18 \times 0.20 \times 0.40$	$0.08 \times 0.10 \times 0.22$
Crystal morphology	Prism	Prism	Prism	Prism
Temperature [K]	160(1)	160(1)	160(1)	160(1)
Crystal system	Monoclinic	Triclinic	Triclinic	Triclinic
Space group	$P2_1/n$	$P\bar{1}$	$P\bar{1}$	$P\bar{1}$
a [Å]	10.31062(19)	9.1931(3)	8.2963(2)	8.1462(2)
b [Å]	12.9030(3)	9.3905(2)	9.1120(3)	9.7827 (2)
c [Å]	11.14250(18)	9.6450(3)	10.5952(3)	10.9351(2)
α[°]	90	75.504(2)	85.548(2)	82.3929(14)
β[°]	93.2024(16)	82.229(2)	88.100(2)	86.3120(12)
γ[°]	90	86.996(2)	84.163(2)	81.9878(11)
V [Å^3]	1480.06(5)	798.57(4)	794.14(4)	854.40(3)
Z	2	1	2	2
D_x [g cm^{-3}]	2.296	2.497	2.511	2.700
μ[mm^{-1}]	10.786	14.680	14.762	12.646
Transmission factors [min, max]	0.33, 1.00	0.065, 0.28	0.035, 0.17	0.13, 0.46
θ range[°]	3–29	3–29	3–29	2–30
Reflections measured	11742	12326	12018	20855
Independent reflections; R_{int}	3242; 0.026	3511; 0.049	3504; 0.056	4962; 0.065
Reflections with $I > 2\sigma(I)$	2729	3140	3215	4456
Number of parameters	192	192	192	192
$R(F)$ [$I > 2\sigma(I)$]	0.020	0.029	0.036	0.029
$wR(F^2)$ [all data]	0.044	0.057	0.078	0.070
GOF(F^2)	1.005	1.033	1.081	1.090
$\Delta\rho_{max, min}$ [e Å^{-3}]	1.78, -0.78	0.99, -1.30	1.92, -2.37	1.37, -2.18

683

684 **Table 3**

685 Selected bond lengths [Å] and angles [°] for **1**-**10**[a].

	1[b]	**2**[b]	**3**[b]	**4**	**5**	**6**	**7**	**8**	**9a**	**9b**	**10**
Hg(1)-N(1)	2.354(6)	2.288(6) 2.295(6)	2.404(5)	2.343(5)	2.300(3)	2.329(5)	2.342(5)	2.262(3)	2.391(4)	2.344(4)	2.375(3)
Hg(1)-N(2)	2.490(6)	2.471(5) 2.467(5)	2.438(5)	2.473(5)	2.513(3)	2.488(5)	2.554(5)	2.535(3)	2.531(3)	2.401(4)	2.458(3)
Hg(1)-X(1)	2.423(2)	2.5010(7) 2.4994(7)	2.6698(5)	2.4572(19)	2.4987(10)	2.4762(17)	2.4106(16)	2.5490(8)	2.5128(5)	2.4996(6)	2.6721(3)
Hg(1)-X(1')	3.011(2)	3.4749(8) 3.6344(8)	-	2.9254(17)	3.0172(10)	2.9343(16)	3.2330(15)	2.8929(7)	3.3759(5)	-	-
Hg(1)-X(2)	2.355(3)	2.5779(7) 2.5831(7)	2.6363(5)	2.371(2)	2.3651(11)	2.3774(18)	2.3990(15)	2.3876(9)	2.4740(6)	2.5168(6)	2.6559(3)
N(1)-Hg(1)-N(2)	70.3(2)	71.13(18) 71.30(18)	69.73(18)	70.28(18)	71.00(11)	70.05(18)	69.05(16)	70.42(9)	68.40(11)	71.24(13)	69.75(10)
N(1)-Hg(1)-X(1)	107.73(16)	144.52(13) 141.55(14)	104.46(13)	104.54(14)	104.08(9)	102.06(14)	121.87(12)	102.46(7)	107.82(9)	115.77(10)	105.10(7)
N(1)-Hg(1)-X(2)	113.76(17)	96.39(13) 100.57(14)	114.29(14)	122.60(15)	133.29(9)	126.51(14)	97.36(12)	148.09(7)	106.50(9)	106.52(10)	112.21(7)
N(2)-Hg(1)-X(1)	94.10(15)	107.83(12) 108.38(12)	101.71(12)	92.88(13)	95.20(8)	91.84(13)	86.24(11)	101.21(6)	95.60(8)	111.44(9)	114.94(7)
N(2)-Hg(1)-X(2)	104.98(15)	111.26(12) 113.72(12)	114.55(12)	103.86(13)	105.95(8)	107.44(13)	128.18(11)	104.19(7)	106.34(8)	121.52(9)	112.52(7)
N(1)-Hg(1)-X(1')	87.45(16)	74.98(13) 74.97(13)	-	88.23(14)	86.63(8)	87.90(14)	81.82(12)	89.20(7)	87.17(8)	-	-
N(2)-Hg(1)-X(1')	156.50(16)	130.20(13) 129.66(12)	-	157.94(13)	156.85(8)	157.51(13)	134.99(12)	157.83(7)	154.48(8)	-	-
X(1)-Hg(1)-X(2)	138.07(11)	115.66(3) 113.36(3)	133.685(17)	132.82(9)	122.44(4)	131.21(7)	136.59(6)	109.41(3)	144.169(18)	120.02(2)	127.047(10)
X(1)-Hg(1)-X(1')	85.66(7)	80.75(2) 77.54(2)	-	87.62(5)	84.28(3)	88.42(5)	80.82(5)	91.41(2)	84.638(13)	-	-
X(2)-Hg(1)-X(1')	90.34(7)	107.78(2) 108.31(2)	-	91.72(6)	93.59(3)	88.96(5)	87.86(5)	88.37(2)	87.056(15)	-	-
Hg(1)-X(1)-Hg(1')	94.34(7)	98.70(2) 102.94(2)	-	92.38(5)	95.72(3)	91.58(5)	99.18(5)	88.59(2)	95.362(13)	-	-

686 [a] All compounds except **3**, **9b** and **10** are binuclear compounds in which the two halves are related by a

687 crystallographic centre of inversion. Primed atoms indicate the longer Hg···X bridging distance to the second

688 half of the dimer.

689 [b] Data taken from the previously published crystal structures shown in Scheme 1a (compounds **1**-**3**), see ref.6.

690
691

692

693 **Legends to Schemes and Figs.**

694 Scheme 1a. Various structural motifs (**i**-**iv**) observed in mercury(II) compounds with (*E*)-*N*-(pyridin-2-
695 ylmethylidene)arylamine, L (taken from ref. 6).

696

697 Scheme 1b. The L ligands used and the investigated compounds **4**-**10**.

698

699 Fig. 1. UV–Vis spectra of compounds **1**-**10** in acetonitrile (concentration 10^{-5}M). Spectra of
700 compounds **7** and **8**, with CO_2CH_3 substituents, are shown separately for convenience.

701

702 Fig. 2. Fluorescence spectra of compounds **1**-**10** in acetonitrile (concentration ~10^{-5}M) obtained
703 by excitation at the respective absorption maxima (refer to Table 1). Spectra of compounds **7** and
704 **8**, with CO_2CH_3 substituents, are shown separately for convenience.

705

706 Fig. 3. Perspective view of binuclear $[HgCl_2L^1]_2$ **4**. Displacement ellipsoids are drawn at the 30%
707 probability level and unlabelled atoms are related by the symmetry operation 1-x, 1-y, 1-z.

708

709 Fig. 4. Perspective view of binuclear $[HgCl_2L^2]_2$ **5**. Displacement ellipsoids are drawn at the 50%
710 probability level and unlabelled atoms are related by the symmetry operation -x, -y, -z.

711

712 Fig. 5. Perspective view of binuclear $[HgCl_2L^3]_2$ **6**. Displacement ellipsoids are drawn at the 30%
713 probability level and unlabelled atoms are related by the symmetry operation -x, 1-y, -z.

714

Fig. 6. Perspective view of binuclear $[HgCl_2L^5]_2$ **8**. Displacement ellipsoids are drawn at the 30% probability level and unlabelled atoms are related by the symmetry operation -x, 1-y, -z.

Fig. 7. Perspective view of binuclear $[HgBr_2L^5]_2$ **9a**. Displacement ellipsoids are drawn at the 50% probability level and unlabelled atoms are related by the symmetry operation 1-x, 1-y, 1-z.

Fig. 8. Perspective view of mononuclear $[HgBr_2L^5]$ **9b**. Displacement ellipsoids are drawn at the 50% probability level.

Fig. 9. Perspective view of mononuclear $[HgI_2L^5]$ **10**. Displacement ellipsoids are drawn at the 50% probability level.

Fig. 10. Perspective view of binuclear $[HgCl_2L^4]_2$ **7**. Displacement ellipsoids are drawn at the 30% probability level and unlabelled atoms are related by the symmetry operation -x, -y, -z.

Fig. 11. View in projection down the a-axis of the unit cell contents of $[HgCl_2L^1]_2$ **4**. The C–H...π(chelate) [C14–H14c...$Cg(HgN_2C_2)^i$ = 2.82 Å, C14...$Cg(HgN_2C_2)^i$ = 3.743(14) Å, angle at H14c = 162° for symmetry operation i: ½+x, ½-y, -½+z] and π...π [Cg(N1,C1-C5)...$Cg(C7\text{-}C12)^{ii}$ = 3.834(5) Å, angle of inclination = 10.8(4)° for ii: -1+x, y, z] interactions are shown as purple and orange dashed lines, respectively.

Fig. 12. View in projection down the b-axis of the unit cell contents of $[HgCl_2L^2]_2$ **5**. The C–H...π(chelate) [C14–H143...$Cg(HgN_2C_2)^i$ = 2.81 Å, C14...$Cg(HgN_2C_2)^i$ = 3.652(5) Å, angle at H143 = 144° for symmetry operation i: -x, 1-y, 1-z], π...π [Cg(N1,C1-C5)...$Cg(C7\text{-}C12)^{ii}$ =

738 3.636(2) Å, angle of inclination = 1.3(2)° for ii: -x, 1-y, -z; Cg(C7-C12)...Cg(C7-C12)^{iii} =
739 3.599(2) Å, for iii: -x, 1-y, 1-z], C–H...O [C3–H3...O1^{iv} = 2.53 Å, C3...O1^{iv} = 3.457(5) Å, angle
740 at H3 = 167° for iv: 1+x, y, -1+z] and C–H...Cl [C4–H4...Cl2^{v} = 2.77 Å, C4...Cl2^{v} = 3.616(5) Å,
741 angle at H4 = 169° for v: 1-x, -y, -z; C6–H6...Cl1^{ii} = 2.75 Å, C4...Cl2^{v} = 3.639(4) Å, angle at H6
742 = 155°] interactions are shown as purple, orange, blue and brown dashed lines, respectively.
743
744 Fig. 13. View in projection down the c-axis of the unit cell contents of [$HgBr_2L^5$]$_2$ **9a**. The π...π
745 [Cg(N1,C1-C5)...Cg(C7-C12)^{i} = 3.705(3) Å, angle of inclination = 9.0(2)° for i: 1-x, 1-y, -z;
746 Cg(C7-C12)...Cg(C7-C12)^{ii} = 3.706(3) Å, for ii: -x, 1-y, -z], C–H...O [C3–H3...O1^{iii} = 2.32 Å,
747 C3...O1^{iii} = 3.119(6) Å, angle at H3 = 142° for iii: 1+x, -1+y, z] and C−H...Br interactions [C4–
748 H4...Br2^{iv} = 3.04 Å, C4...Br2^{iv} = 3.936(5)Å, angle at H4 = 157° for iv: 1-x, -y, 1-z; C6–H6...Br1^{i}
749 = 3.05 Å, C6...Br1^{i} = 3.903(4)Å, angle at H6 = 150°] interactions are shown as orange, blue and
750 brown dashed lines, respectively.
751
752 Fig. 14 (a) View of the supramolecular chain aligned along the a-axis in [$HgBr_2L^5$]$_2$ **9a**. (b) View
753 in projection down the a-axis of the unit cell contents, highlighting the stacking of layers along
754 the b-axis. The π...π [Cg(N1,C1-C5)...Cg(C7-C12)^{i} = 3.687(3) Å, angle of inclination = 9.7(2)°
755 for i: 1-x, 1-y, 1-z; Cg(HgN_2C_2)...Cg(C7-C12)^{ii} = 3.880(3) Å, angle = 9.2(2)° for ii: -x, 1-y, -z],
756 C−H...O [C5–H5...O1^{iii} = 2.28 Å, C5...O1^{iii} = 3.083(7) Å, angle at H5 = 142° for iii: 1+x, y, -
757 1+z] and C−H...Br interactions [C6–H6...Br2^{i} = 2.91 Å, C6...Br2^{i} = 3.632(5)Å, angle at H6 =
758 134°] interactions are shown as orange (pink for chelate ring), blue and brown dashed lines,
759 respectively.
760

Fig. 15. (a) View of the supramolecular layer in $[HgCl_2L^4]_2$ **7**. (b) View in projection down the a-axis of the unit cell contents, highlighting the stacking of layers along the a-axis and the C–H...Cl connections between them. The π...π [Cg(HgN_2C_2)...Cg(C7-C12)^{i} = 3.821(3) Å, angle of inclination = 3.2(2)° for i: 1-x, -y, 1-z], C–H...O [C3–H3...O1^{i} = 2.60 Å, C3...O1^{i} = 3.418(7) Å, angle at H3 = 146°; C11–H11...O1^{ii} = 2.54 Å, C11...O1^{ii} = 3.291(8) Å, angle at H3 = 136° for ii: x, ½-y, -½+z] and C–H...Cl [C6–H6...Cl2^{iii} = 2.73 Å, C6...Cl2^{iii} = 3.559(6) Å, angle at H5 = 146° for iii: 1+x, y, z; C9–H9...Cl1^{iii} = 2.81 Å, C9...Cl1^{iii} = 3.558(7) Å, angle at H5 = 136°] interactions are shown as orange, blue and brown dashed lines, respectively.

Synthesis, crystal structures and optical properties of mercury(II) halide compounds with (*E*)-*N*-(pyridin-2-ylmethylidene)arylamine: Effect of ligand R-group upon structure

Tushar S. Basu Baul[a,*], Sajal Kundu [a], Herbert Höpfl[b], Edward R. T. Tiekink[c,*], Anthony Linden[d]

Graphical Abstract (Picture)